IEEE Access
Multidisciplinary ⋮ Rapid Review ⋮ Open Access Journal

Received 10 August 2024, accepted 26 August 2024, date of publication 29 August 2024, date of current version 10 September 2024.

Digital Object Identifier 10.1109/ACCESS.2024.3451535

RESEARCH ARTICLE

Operation Strategy for a Stand-Alone Hybrid Energy System Supplying a Remote Residential Home for Minimizing Total Cost and Carbon Emission Equipped With Geothermal System

HIBA ABDULKAREEM KHAMIS[1], ELAHEH MASHHOUR[1], (Member, IEEE), MAHMOOD JOORABIAN[1], SEYYED GHODRATOLLAH SEIFOSSADAT[1], AND SALMAN H. HAMMADI[2]

[1]Department of Electrical Engineering, Faculty of Engineering, Shahid Chamran University of Ahvaz, Ahvaz 61357-83151, Iran
[2]Department of Mechanical Engineering, Engineering College, Basrah University, Basrah 61004, Iraq

Corresponding author: Elaheh Mashhour (e.mashhour@scu.ac.ir)

This work was supported by the Research Council of Shahid Chamran University of Ahvaz under Grant SCU.EE1401.197.

ABSTRACT This study deals with the operational control strategy of a Hybrid System (HS) for a residential home equipped with a Geothermal System (GS). HS includes photovoltaic (PV), wind turbine (WT), battery energy storage system (BESS), and diesel generator (DG). The thermodynamic module of the GS was used to calculate the value of the electrical energy that could be saved, and the variation in environmental temperature during the day was considered. The presented model was studied using different scenarios for a residential home in Iraq and analyzed in terms of economic and environmental aspects. The results show that during some hours of the day, a GS minimizes the power drawn from the DG, reducing the cost and emissions of the total electrical power generation.

INDEX TERMS Solar energy, wind turbine, battery, diesel generator, geothermal system.

NOMENCLATURE

ABBREVIATIONS

HS	Hybrid System.
PV	Photovoltaic.
WT	Wind Turbine.
DG	Diesel Generator.
GS	Geothermal System.
RE	Renewable Energy.
HRES	Hybrid Renewable Energy System.
BESS	Battery Energy Storage System.
SOC	State of Charge.
EAHE	Earth-to-Air Heat Exchanger.
UHE	Underground Heat Exchanger.
TR	Ton of Refrigeration.
CO_2	Carbon Dioxide.

PARAMETERS, CONSTANTS, AND VARIABLES

A_{PV}	Array Area, m^2.
R	Rotor Blade Radius, m.
t	Time of Generation, hour.
C_p	Power Coefficient.
IC	Initial Cost, \$.
i	Interest Rate, %.
CF_{wt}	WT Capacity Factor.
Com_{wt}	Operation and Maintenance Cost, \$.
t	Time of Generation, hour.
$C_{rep,bat}$	Battery Replacement Cost, \$.
N_{bat}	Number of Batteries.
C''_{bat}	Battery Nominal or Rated Capacity.

The associate editor coordinating the review of this manuscript and approving it for publication was Lei Chen.

B_{bat}	Battery Voltage, V.
P_{DGr}	DG Rated Power, kW.
C_f	Fuel Cost Per Liter, $.
T_m	Soil Temperature, °C.
A_s	Annual Surface Temperature, °C.
z	Vertical Coordinate, m.
D	Pipe Diameter, m.
T_P	Pipe Surface Temperature, °C.
$\dot{m}$	Air Mass Flow Rate, kg/s.
c	Specific Heat of Air, J/kg.
T_i	Output Temperature of UHE, °C.
L	Length of the Pipe, m.
T_o	Outlet Air Temperature, °C.
N_w	Number of Wind Turbines (WT) Installed.
h	Wind Tower Height, m.
r	Radius of Wind Turbine (WT), m.
C_{wf}	Installation and Fabrication Costs of WT.
Y_{proj}	Project Lifetime, years.
M_{year}	Annual Maintenance Cost, $.
N_{year}	Lifetime, year.
C_{pipe}	Pipes Cost, $.
$C_{dr\&cr}$	Cost of Drilling and Creation, $.
C_m	Maintenance Cost, $/ year.
K	Thermal Conductivity of Air.
η_{bat}	Battery Efficiency, %.
ρ	Air Density, kg /m^3.
β	Self-Discharge Rate, %.
δ_C	Temperature Coefficient, % / degree.
η_{inv}	Inverter Efficiency %.
α_D &β_D	Coefficients of Fuel Consumption.
α	Soil Diffusivity, m^2/hr.
μ	Air Viscosity, $kg/m.s$

I. INTRODUCTION

The demand for energy from conventional energy sources has rapidly increased. Traditional energy sources have contributed to meeting electricity demand. Nevertheless, the detrimental consequences associated with the excessive utilization of fossil fuels have become increasingly apparent. The pressing issues of global climate change, energy availability, and increasing emissions that damage the environment necessitate a focused approach toward reducing fossil fuel energy dependency. Renewable energy (RE) sources are the optimal solutions for these issues.

Utilizing RE has many benefits, including the paramount benefit of inherent renewability. RE sources, such as solar, wind, and geothermal, are characterized by their permanent availability and unlimited nature. They offer indisputable health and environmental advantages and are more cost-effective than conventional energy sources.

A stand-alone system is an autonomous unit that produces electricity from a renewable source. Photovoltaic (PV) and wind turbine(WT) directly use electricity to operate electrical loads without depending on the utility grid system. Hence, the challenge is to deal with the increasing worldwide demand for energy while gradually reducing the dependence on fossil fuel resources. Utilizing a hybrid system (HS) is an efficient method to address these issues. PV panels and WT are highly efficient for generating sufficient energy. It is essential to seek economic solutions for expensive matters, particularly for houses in remote regions, where access to basic amenities such as water pumping, cooking, and lighting is needed and where energy is essential for improving the standard of living.

Expanding the power generation system by utilizing renewable sources is necessary to meet this increasing demand. Hybrid renewable energy systems (HRES), such as wind and solar power, offer a viable solution for generating electricity in remote regions. These systems utilize RE sources as the primary means of power production, resulting in a supply of affordable electricity. Akram et al. [1] introduced an improved strategy to optimize the capacity of a standard home microgrid that utilizes distributed RE sources, such as PV and WT, combined with diesel generation (DG) and a battery energy storage system (BESS). Kiros et al. [2] presented a model for an autonomous HS designed for the remote regions of Ethiopia. In addition, a comparison was made regarding the economic performance of different scenarios for an autonomous hybrid (PV-WT). This system includes battery storage and a DG as a backup for providing electricity to remote rural areas. Abdullah et al. [3] developed a method to reduce the variability in wind power generation and the effect of RE resource intermittency focusing on scaling hybrid (PV -WT) power systems. Fernández-Muñoz and Pérez-Díaz [4] proposed a set of two optimization models designed for the efficient scheduling and dispatch of a virtual power plant consisting of a wind farm and Li-ion battery in the short term. Muhammad et al. [5] presented an optimal planning approach for a hybrid (hydro-PV-DG-BESS). They used a dynamic programming technique to achieve this goal. Velasco de la Fuente et al. [6] studied a solar power management system combined with a battery that could operate autonomously or be connected to a grid. Ogunjuyigbe et al. [7] employed a genetic algorithm to optimize a multi-objective model for a grid-autonomous hybrid energy system. This system comprises a (PV-WT-BESS-DG). Zhang et al. [8] analyzed the current financial incentive schemes for combined PV energy and BESS. Nurunnabi et al. [9] performed a feasibility and sensitivity analysis of off-grid and grid-connected microgrids powered by RE. They focused on the possibility of using wind and solar energy in various regions of Bangladesh. The optimum HRES designs combining (WT, PV, grid, and battery) for the specified region were determined. Moghaddam et al. [10] presented a design for an efficient HRES that combines PV, WT, and BESS. Their systems aimed to improve the reliability of the load supply during a specific analysis period. Esan et al. [11] performed a design and techno-financial analysis of a hybrid mini-grid system containing a PV array, diesel generators(DGs), and battery storage. They also verified the reliability of the simulation results obtained using HOMER software for a typical rural community in

Nigeria. Diab et al. [12] proposed a simulation model that accurately represents the operation of a hybrid microgrid system containing (PV-WT-DG) and battery bank storage. Razmjoo et al. [13] studied the possibility of achieving energy sustainability in two highly potential cities in southeastern Iran by utilizing RE sources until 2030. Homer software was employed to calculate (PV-WT-DG) HS economical and technical analyses. In 2020, de Freitas Moscardini Júnior and Rüther [14] evaluated the variations in outcomes resulting from using five different solar irradiation databases to size hybrids (PV-DGs). These generators were designed to provide electricity to isolated mini-grids. Nsafon et al. [15] focused on the sustainability and techno-economic viability of a hybrid (PV-WT-DG) system intended for a distributed power supply. Covic et al. [16] analyzed the investment decision to use BESS-PV in an uncertain industrial plant to determine the optimal investment capacity. Medina and Lata-García [17] presented a series of simulations to evaluate the feasibility of implementing an isolated system. They investigated economic and technological requirements to determine the most cost-effective and competitive energy solutions. Their study focused on an HS combined with PV and WT systems using BESS. Mulenga et al. [18] studied the viability of using (PV-DG) to provide electricity to rural areas, using a case study of the Chilubi region in Zambia. Mikati et al. [19] presented the results of modeling a distributed small-scale power system. This system includes demand power, solar arrays, small-scale WT, and grid connections. Sharma and Bhatti [20] introduced a method for automatically controlling the reactive power of isolated (WT-DG) hybrid power systems. These systems consist of a permanent magnet induction generator for wind energy conversion and a synchronous generator for a DG set. Badwawi et al. [21] comprehensively analyzed the difficulties and potential solutions associated with combining solar and wind energy sources to generate electricity. Sachs and Sawodny [22] developed an advanced control technique for managing microgrids with hybrid island energy systems. An island energy system comprising DG, PV, and a battery was the microgrid type considered in their study. Mangu et al. [23] proposed a control technique to achieve power flow in a grid-connected system that combines PV, WT, and battery technologies. Yi et al. [24] introduced the control and management of power systems for PV-battery-based hybrid microgrids. This system can be operated in both the grid-connected and islanded modes. Mbungu et al. [25] developed a model predictive control method to manage energy and efficiently control the hybrid (PV – WT- battery-grid) power system. Sawle et al. [26] proposed the concept of utilizing a PV-WT-battery and DG systems to study different configurations, control strategies, techno-economic analyses, and social effects. Gatta et al. [27] comprehensively analyzed the implementation of a hybrid power plant on Giglio Island. This power plant combines PV technology, lithium batteries, and synchronous condenser systems to replace current diesel units. Tiwari et al. [28] introduced a wind energy system incorporating DG and BESS. Through its control system, the proposed system manages the loading of DG to achieve a reduced specific fuel consumption. García-Sánchez et al. [29] presented a controller method for a small WT that operates at varying speeds and is connected to a grid. Their scheme focuses on tracking the maximum power point. Singh et al. [30] utilized a PV array, BESS, DG, and a grid connection. Juma et al. [31] introduced a microgrid that utilizes distributed energy resources to power a stand-alone system in a rural area. The system consists of (PV-BESS and WT) connected to a permanent magnet synchronous generator. Al-Quraan and Al-Qaisi [32] developed and supervised an autonomous microgrid system comprising a PV and WT energy conversion system using a permanent magnet synchronous generator. Ez-zahra Lamzouri et al. [33] proposed a novel robust control method that relies on an energy management strategy for an autonomous HS. They include a wind energy conversion system, PV energy generation system, and battery bank. Thirugnanam et al. [34] introduced a battery energy management system for microgrids. Their system primarily depends on PV panels and DGs as the main sources of electricity. Eltamaly et al. [35] presented a model and simulation of a smart grid that incorporated hybrid energy systems, batteries, and DG. The purpose of their study was to use a grid to provide power to an isolated load in a rural area in the northern region of Saudi Arabia. In 2023, Liu et al. [36] developed and demonstrated a novel technique using a BESS to enhance the Automatic Generation Control performance of wind farms. Gulzar et al. [37] analyzed and managed a hybrid grid-connected system. They combined a (WT-PV- BESS) with a Fuel Cell for enhanced efficiency and control. Fan et al. [38] presented the impact of many parameters on the heat exchange rate, including depth, thermal features, inlet temperature, mass flow, and length of the geothermal heat exchanger. In 2009, Nayak and Tiwari [39] simplified a mathematical model to analyze the efficiency of a PV-thermal system and an earth-air heat exchanger (EAHE) combined with a greenhouse in Delhi, India. Chel and Tiwari [40] conducted an experimental study to evaluate the performance of a PV–operated EAHE. Congedo et al. [41] explored the thermal effects of ground source heat pumps with a horizontal heat exchanger on soil that comes in contact with the ground. Loveridge and Powrie [42] developed a ground heat exchanger connected to a ground source heat pump and actively regulated it to maintain the building temperature within the desired comfort range. Jakhar et al. [43] assessed the thermal efficiency of an earth-to-air tunnel heat exchanger combined with a duct for solar-air heating. The purpose was to heat the air in Ajmer City's arid climate during winter. Ajmer City is located in Northwest India. Soni et al. [44] reviewed experimental and modeling investigations conducted using ground-coupled heat exchanger systems. Kaushal et al. [45] analyzed the thermal performance of a 2D hybrid earth-to-air tunnel heat exchanger. Wang et al. [46] proposed an analytical comparison between horizontal

geothermal heat exchangers and vertical spiral coils coupled with heat pumps. Boughanmi et al. [47] estimated the thermal effectiveness of a novel geothermal heat exchanger called the conical basket geothermal heat exchanger. The purpose of this heat exchanger is to provide both cooling and heating to the greenhouses. Elminshawya et al. [48] studied the technological viability of combining an EAHE with a PV module to create a geothermal cooling system to regulate the average cell temperature and enhance PV module performance. Naseh and Behdani [49] introduced a technique to determine the optimum efficient parameters for a hybrid (PV- WT-DG - geothermal system (GS)) system for off-grid and grid-connected configurations. Amanowicz and Wojtkowiracteak [50] implemented a study that examined how different airflow distribution designs affect the thermal performance of a multi-pipe EAHE, aiming to fill the gap in this area of research. Ahmed et al. [51] conducted a comprehensive review of the existing literature on modeling techniques for EAHE used in buildings. They specifically focused on physical and hybrid approaches, and discussed the potential advantages, developments, and difficulties associated with these techniques. Xiong et al. [71] introduced some assumptions to facilitate the modeling and simulation of the coupled thermo-hydro process throughout geothermal development in an enhanced GS because of the rapid depletion of geothermal energy. In addition, a high injection temperature can improve the lifetime of power generation under the same injection pressure.

The literature survey shows that HS has been the focus of researchers in recent decades, and there are valuable works dealing with different aspects of these systems, including the planning, operation, and control of the system. Previous studies have focused on components such as PV systems, WTs, BESS, and DGs as backup systems. However, few studies have considered GS by focusing on work concentrated on the structure of geothermal systems (GSs) and their thermal performance. As mentioned earlier, RE sources are favored because of their impact on reducing greenhouse gas emissions; however, they are not continuous sources and backup systems are inevitable. GS can effectively reduce the need for a DG or any generation unit based on fossil fuels. Nonetheless, less attention has been paid to the impact of GS on the electrical subsystem planning of an HS. To the best of our knowledge, the thermodynamic behavior of a GS is not considered for the operational planning of an HS; this study aims to address this gap by using an HS including a PV, WT, battery, and DG for a residential home equipped with a GS located in Basrah City, a southern region of Iraq.

The main contributions of the current Research are as follows:

1. The operational planning of an HS is studied, considering the impact of a GS on reducing electrical consumption.

2. The advantage of a GS in operating an HS with less cost and avoiding the environmental pollution effect of using a DG is that the thermodynamic behavior of the GS is considered. To the best of our knowledge, researchers have not yet focused on this topic.

3. The energy savings in the home caused by GS use the thermodynamic model of the GS and the 15-minute operational planning of the HS as inputs. At each 15-minute time interval, the value of energy savings caused by the GS can be updated. Accordingly, home generation units, loads, and batteries are managed in a cost-effective manner.

4. The model's efficiency was demonstrated by various numerical evaluations that validated the impact of GS on reducing greenhouse gas emissions and their associated costs.

The remainder of this paper is organized as follows: Section I presents the introduction and outlines previous research. Section II details the mathematical model of the hybrid power system (PV-WT-BESS-DG-GS). Section III explains the control strategy for HS operation. Section IV presents the numerical results, where many scenarios were simulated using MATLAB programming for residential load operation. In addition, this section describes the simulation of electrical power generation with and without a GS. Section V estimates the economic valuation of the results and calculates the cost and emissions of electrical power generation sources for both summer and winter. Finally, conclusions are presented in Section VI.

II. MATHEMATICAL MODEL OF HYBRID POWER SYSTEM

The proposed system contains a stand-alone HS (in this study, we used a PV-WT with batteries and DG as backup sources equipped with a GS to feed the electrical loads for a home in a remote area in Basrah City in the southern region of Iraq.

A. PHOTOVOLTAIC SYSTEM

The effects of the total solar insolation and ambient temperature of the site were carefully incorporated to calculate the output power of the PV array [52]. The total amount of solar generation, measured in kWh, is determined as [53]:

$$P_{PV} = \eta_{PV} \times A_{PV} \times G_A \times (1 - 0.005 \times (T_{amb} - 25)) \quad (1)$$

where P_{PV} is the output power of the PV in kW, η_{PV} is the conversion efficiency of the PV array in percentage, A_{PV} is the area of the array in m^2, G_A is the solar radiation in kW/m^2, and T_{amb} is the outside air temperature in °C. It was assumed that the entire radiation was directed toward the PV array without considering the angle of incidence.

B. WIND TURBINE SYSTEM

The WT power output depends on the wind speed and is calculated as (2):

$$P_{WT} = 0.5 \times \rho \times A \times V^3 \quad (2)$$

where P_{WT} is the output power of the WT in kW, ρ is the air density in kg/m^3, and A is the area covered by the blades of the WT in m^2. The formula for A is given by $A = \pi R^2$ [67], where R is the radius of the rotor blade in m, and V represents the wind speed in m/s [54].

The mechanical power generated by WT at time t is shown below:

$$P_{WT}(t) = \begin{cases} 0 & V \le V_{ci} \\ P_r \times \left(\left(V^3(t) - V_{ci}^3\right) / \left(V_r^3 - V_{ci}^3\right)\right) & V_{ci} \le Vb \le V_r \\ P_r & V_r \le V \le V_{co} \\ 0 & V_{co} \le V \\ P_r = 0.5 \times C_p \times \rho \times A \times V^3 & \end{cases} \tag{3}$$

where V_{ci}, V_{co}, and $V_r V_r$ are cut-in, cut-out, and rated wind speed, in *m/s,* respectively, P_r is the rated power, and C_p is the power coefficient, the values of V_{ci}, V_{co}, and V_r are 2.3 m/s, 9 m/s, and 2.9 m/s respectively [54]. Wind speed was obtained from meteorological data in the Basrah region [56].

C. BATTERY SYSTEM

Battery banks in hybrid PV-WT systems are electrochemical devices designed to store energy from various AC or DC sources for future utilization. The batteries operate as a backup system to provide energy for the load operation if the power from the PV and WT is insufficient to satisfy the load demand. It is necessary to satisfy the following constraints to determine the state of charge (SOC) of an energy storage device:

$$SOC_{min} \le SOC \le SOC_{max}$$

where SOC_{max} and SOC_{min} are the maximum and minimum charge states, respectively. This study assumes that SOC_{min} and SOC_{max} are equal to 50% and 80%, respectively. The battery bank has a specified nominal capacity in ampere-hours that can supply energy to the load until it reaches the maximum depth of discharge or minimum SOC, as indicated in [57]. The variations in battery capacity may often be expressed by utilizing the temperature coefficient δ_c as follows:

$$C'_{bat} = C''_{bat} \times (1 + \delta_c \times (T_{bat} - 298.15)) \tag{4}$$

where C'_{bat} is the battery capacity in Ah, C''_{bat} the battery-rated capacity refers to the capacity value provided by the manufacturer as the standard value that identifies the characteristics of the battery in Ah, δ_C is the temperature coefficient that measures the temperature change of the battery and T_{bat} is the battery temperature in °Cy. The SOC of the battery at time t + 1 can be determined as [58]:

$$SOC(t+1) = SOC(t) \times \left(1 - \frac{\beta \times \Delta t}{24}\right) + \frac{P_{bat} \times \Delta t \times \eta_{bat}}{\eta_{inverter} \times C'_{bat} \times B_{bat}} \tag{5}$$

where $SOC(t+1)$ represents the SOC in percentage of the battery in time (t+1), $SOC(t)$ is the previous battery state of charge in percentage, β is the rate of self-discharge in percentage, which depends on the battery state of health and the accumulated charge, P_{bat} is the power taken from the battery (if $P_{solar-wind} > P_{load}$ then P_{bat} is +ve else P_{bat} is –ve) in kW, η_{bat} is the battery efficiency in percentage, η_{inv} is the inverter efficiency in percentage, C'_{bat} is the battery capacity in Ah, and B_{bat} is the battery voltage in *volt*.

D. DIESEL GENERATOR

The DG activation and dispatch pattern is employed to satisfy the residual load demand, that is, the load part not supplied by the PV, WT, and BESS [59]. The final decision is made due to the high cost of the fuel and its production of greenhouse gases, specifically carbon dioxide (CO_2). The benefit of utilizing a DG lies in its ability to operate at any time of the day according to the demand. The constraint on the energy generated by the DG is $0 \le P_{DG}(k) \le P_{DG}^{max}$ [60].

A DG is the conventional energy source used as a backup system to supply power with an HRES. The fuel consumption of DG per hour is evaluated as:

$$D_f(t) = \alpha_D \times P_{DG}(t) + \beta_D \times P_{DGr} \tag{6}$$

where $D_f(t)$ is the fuel consumption of the DG in *liter/h*, P_{DG} represents the average power of the DG in kW, P_{DGr} represents the rated power of the DG in kW, α_D and β_D are the fuel consumption curve coefficients [61].

E. GEOTHERMAL SYSTEM

The innovation of this work is related to the use of GS to reduce load power consumption. In hot and cold climate regions, most of the electricity required for residential buildings is used for heating and cooling. Figure 1 shows the hybrid (PV-WT-DG and BESS) equipped with a GS.

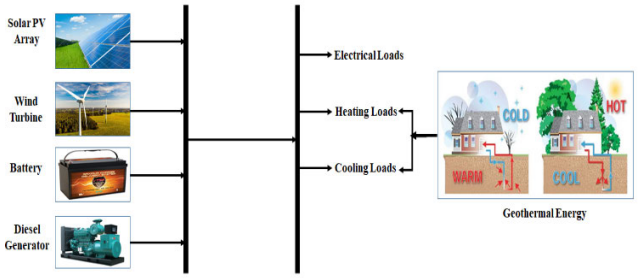

FIGURE 1. The architecture of hybrid PV-WT –BESS- DG with GS.

An underground heat exchanger (UHE) is used to reduce the energy required for the cooling or heating processes. The UHE absorbs heat from the soil for heating and dissipates heat into the soil for cooling. When high-temperature air enters the UHE, it exchanges heat with the soil, gradually decreasing the air temperature to a value close to the soil temperature, depending on the length of the heat exchanger. Previous studies in some Middle Eastern countries have shown that a UHE reduces the cooling load by approximately 30%. This indicates that when air passes through a buried EAHE pipe in winter, it produces a heating effect, and in summer, it produces a cooling effect. The working principle of the EAHE system is illustrated in Figure 2.

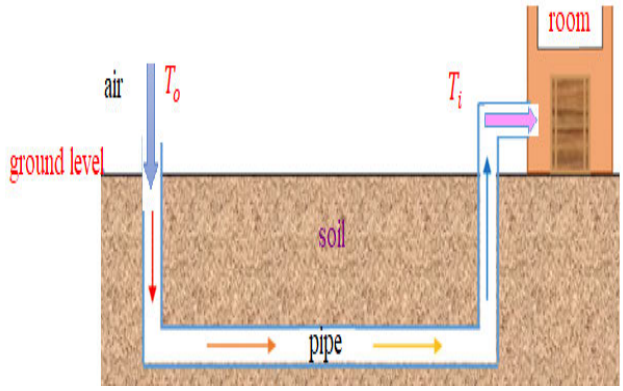

FIGURE 2. Working principle of the EAHE system.

The soil temperature as a function of soil depth and time is given by [62].

$$T(z.t) = T_m - A_s \times Exp\left[-z\times\left(\frac{\pi}{8760\times\alpha}\right)^{0.5}\right] \times cos\left[\frac{2\times\pi}{8760}\times\left[t - t_o - \frac{z}{2}\times\left(\frac{8760}{\pi\times\alpha}\right)^{0.5}\right]\right] \tag{7}$$

where $T(z.t)$ is the soil temperature in °C, T_m is the annual mean ground temperature in °C, A_s is the annual surface temperature in °C, z is the vertical coordinate in m, α is the soil diffusivity in $m^2/hr.$, t is the time in $hr.$, and t_o is the phase constant in $hr.$, as shown in Figure 3.

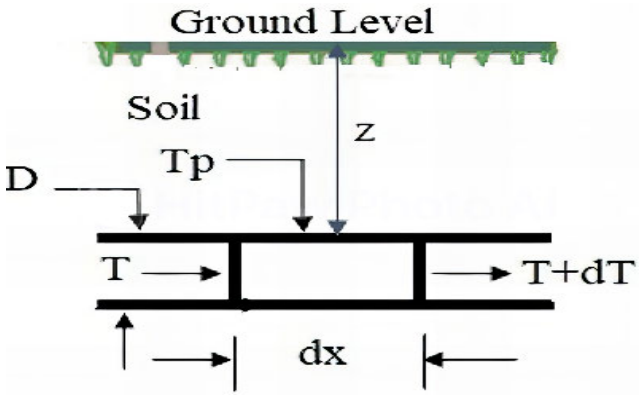

FIGURE 3. EAHE system parameters.

The heat balance of the UHE is given below:

$$h\times\pi\times D\times(T - T_P)\,dx = -\dot{m}\times c\times dT \tag{8}$$

Where h is the heat transfer coefficient in $w/m^2.$°C, D is the pipe diameter in m, T is the air temperature in °C, T_P is the pipe surface temperature in °C, $\dot{m}$ is the air mass flow rate in kg/s, and c is the specific heat of the air in J/kg.

The heat transfer coefficient and its value depend on the amount of flow and can be calculated using Equation (9).

$$h = \frac{NU\times bK}{D} \tag{9}$$

where h is the heat transfer coefficient in $w/m^2.$°C, NU is the Nasselt number, K is the thermal conductivity of air in $w/m.$°C, and D is the pipe diameter in m.

$$NU = 0.023\times Re^{0.8}\times Pr^{1/3} \tag{10}$$

where NU, Re, and Pr are the Nasselt, Reynolds, and Prandtle numbers, respectively.

$$Re = \frac{4\times\dot{m}}{\pi\times D\times\mu} \tag{11}$$

where Re is the Reynold's number, $\dot{m}$ is the air mass flow rate in kg/s, D is the pipe diameter in m, and μ is the viscosity of air in $kg/m.$s. Integrating the last equation with the inlet boundary conditions into the final state yields:

$$x = 0 \quad T = T_i$$
$$x = L \quad T = T_o$$

Give the outlet air temperature for any pipe length as:

$$T_o = T_P + (T_i - T_P)\times Exp\left[-h\times\pi\times D\times\frac{L}{\dot{m}c}\right] \tag{12}$$

where T_o is the outlet air temperature that enters the pipe in °C, T_P is the pipe surface temperature in °C, T_i is the inlet temperature to home (the output air temperature from the UHE) in °C, h is the heat transfer coefficient in $w/m^2.$°C, D is the pipe diameter in m, L is the length of the pipe in m, $\dot{m}$ is the air mass flow rate in kg/s, and c is the specific heat of the air in $J/$kg.°C. The energy saved from temperature reduction in the UHE is given by [62].

$$Q = \dot{m}\times c\times(T_o - T_i) \tag{13}$$

where $\dot{m}$ is the air mass flow rate in kg/s, c is the specific heat of the air in $J/$kg.°C., T_o is the temperature of the outside air entering the UHE in °C, and T_i is the inlet temperature to home (the output air temperature from the UHE) in °C, as shown in Figure 2.

III. CONTROL STRATEGY FOR THE OPERATION OF HYBRID SYSTEM

The HS can be divided into three groups in off-grid mode: generation, storage, and load. First, the energy management of the HS depends on the power generated by RE sources PV and WT. Because there are two RE sources, the program will compare the power of the PV and WT, and then select the maximum source to generate electricity and turn on the loads; the rest of the power is used to charge the batteries. If the summation of both RE sources, PV-WT is not sufficient to meet the load demand, here are the benefits of using batteries and DG to meet the required load's power, but it should be taken into account that the battery SOC should not be less than 50% to be used for longevity and to maximize battery lifetime.

As mentioned, the PV array, WT, battery bank, and DG should supply the daily power requirements cooperatively as follows:

$$P_{PV} + P_{WT} + P_{bat} + P_{Diesel} = P_{load} \tag{14}$$

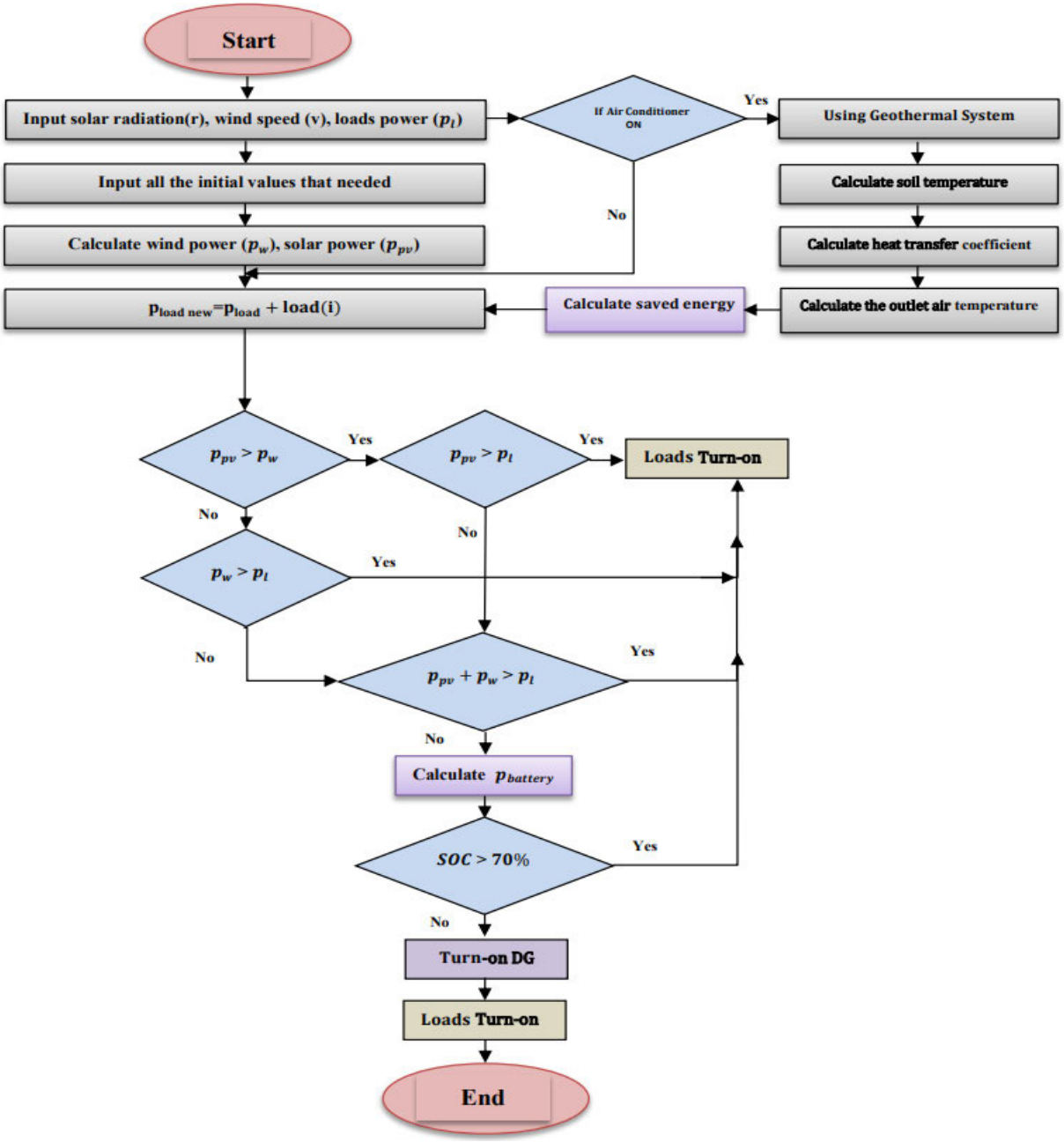

FIGURE 4. Power management of the hybrid PV-WT-BESS- DG.

where P_{PV}, P_{WT}, P_{bat}, P_{Diesel}, and P_{load} are the PV, WT, battery, DG, and load powers, respectively, in kW.

The power summation for all the energy sources should equal or exceed the load consumption. On the other hand, GS can save energy in the home by reducing power consumption (cooling/heating loads).

The proposed loads used in this study are listed in Table 1. The control strategy applied in this study for power management of the hybrid (PV-WT- BESS-DG) is shown in the flowchart in Figure 4, which explains the load control strategy that must be used to turn on the loads concerning the availability of solar radiation and wind speed with the addition of backup batteries and DG. In the supposed HS, only the DG consumes fuel, and the prioritization of the units (PV-WT-BESS-DG) is performed quickly using a simple algorithm, as shown in Figure 4.

IV. NUMERICAL RESULTS

According to the actual data calculated for a sample day on July 13 in Basrah City, a southern region in Iraq, Figures 5 and 6 show the solar radiation and wind speed that will be used to generate PV and WT power energy, whereas Figure 7 shows the hourly load power over one day according to Table 1, which contains the proposed residential loads and

their power consumption. Table 2 lists all the factors used for the numerical calculation obtained from [53], [55], [58], [61], [62], [65], [67], and [68]. Figure 8 shows the hourly ambient temperature measured in Basrah, Iraq, over one day in July.

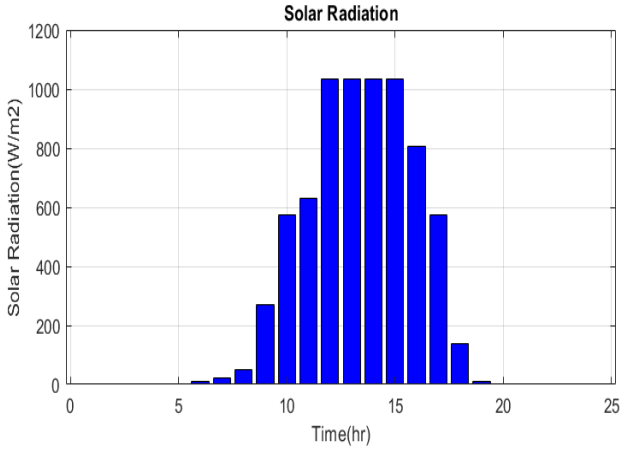

FIGURE 5. Hourly solar radiation for July 13 in Basrah Iraq.

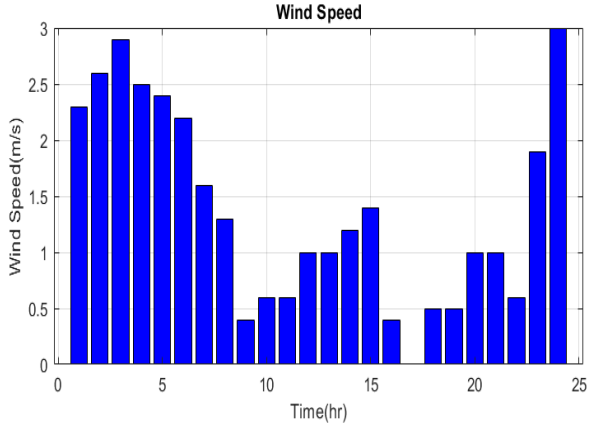

FIGURE 6. Hourly wind speed for July 13 in Basrah Iraq.

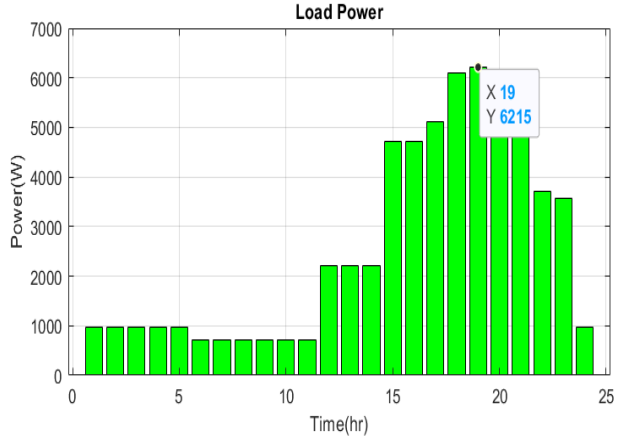

FIGURE 7. Hourly load power over one day.

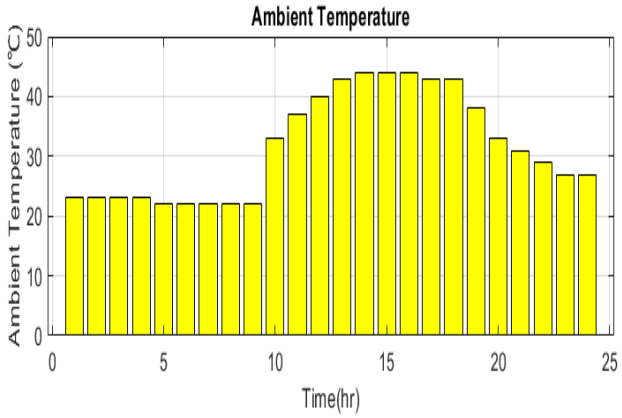

FIGURE 8. Hourly ambient temperature for July 13 in Basrah Iraq.

A. ELECTRICAL POWER GENERATION WITHOUT UTILIZING A GEOTHERMAL SYSTEM

Different scenarios evaluated the proposed control strategy using a hybrid PV-WT energy source with batteries and DG as a backup system. First, these scenarios occurred without a GS.

1) SCENARIO (A): PV-BESS

A PV energy system connected to a battery is the first configuration for turning the loads on. The loads were turned on depending on the PV power generation, which was calculated according to the availability of solar radiation with the addition of backup batteries. Solar radiation started at zero and increased until it reached a maximum value of 1033 w/m^2.

Despite this value, the PV power with a battery as a backup source is severely restricted by the battery SOC level, which must not drop below 50 percent, making it challenging to meet the maximum load demand. Figures 9 and 10 show the PV energy with battery power, which is used as a backup source only when the PV power generation does not meet the load demand, considering that the battery SOC should be greater than 70%.

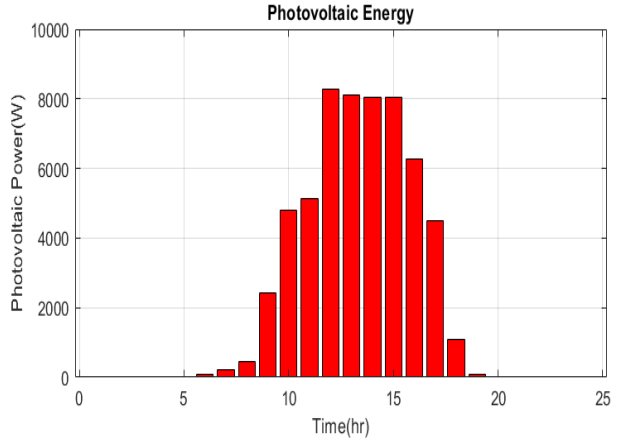

FIGURE 9. PV power generation.

TABLE 1. The proposed electrical loads.

Electrical Appliance	Number	Power consumption (W)	Time of use (h)
Incandescent Lamp	2	200	17:00-22:00
Fluorescent Lamp	1	60	00:00-00:00
Satellite Receiver	1	25	19:00-23:00
Refrigerator	1	400	00:00-00:00
Electric Iron	1	1000	18:00-19:00
Air Conditioner	1	2500	15:00-23:00
Freezer	1	250	00:00-00:00
Television	1	80	19:00-23:00
Cooking Range	1	1500	12:00-21:00
Air Cooler	1	250	23:00-05:00

TABLE 2. Parameters and specifications of the proposed system model.

Parameter	Value	Parameter	Value	Parameter	Value	Parameter	Value
η_{PV}	18	t	8760	$Q_{lifetim}$	10569	Y_{proj}	25
A_{PV}	50	t_o	552	η_{bat}	1	IC_w	2000
ρ	1.183	z	5	C''_{bat}	1000	M_{year}	1000
R	20	D	10	δ_C	0.6	N_{year}	25
C_p	0.4	T_P	27	T_{bat}	50	IC_s	5000
β	0	$\dot{m}$	0.2	$SOC(t)$	70	M_{year}	500
ω_m	27.54	c	1.005	β	0.2	N_{year}	25
I	90000	T_i	50	η_{inv}	92	C_{pipe}	75
i	5	L	50	B_{bat}	24	$C_{dr\&cr}$	150
CF_{wt}	0.35	T_o	40	P_{DGr}	5.6	C_m	10
Com_{wt}	1000	N_w	1	α_D	0.246	Y_{year}	30
t	1	h	52	β_D	0.0814	ΔT	15
$C_{O\&M,bat}$	10 $	r	3	C_f	1.28	μ	1.48 e^{-5}
$C_{rep,bat}$	900 $	C_{wf}	50000$	T_m	27℃	K	0.025
α	0.0038	N_{bat}	40	i	5	A_s	13.3 ℃

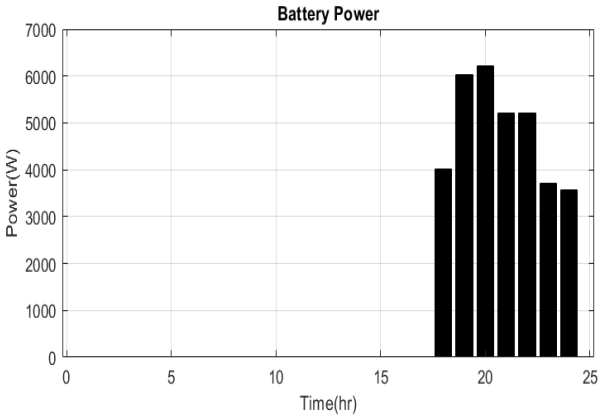

FIGURE 10. Backup battery power.

2) SCENARIO (B): WT-BESS

The second configuration turns on the loads using a wind energy system connected to a battery as an energy storage system. Figures 11 and 12 show that the loads are turned on depending on the wind power generation, which is related to the wind speed availability connected to the backup batteries. The daily wind speed starts at 0.1 m/s and increased progressively until it reached a maximum value of 3 m/s, calculated for a sample day in Basrah on July 13. In addition, this scenario of power generation is not sufficient to turn on all loads, as in Scenario A, because using a battery as a backup source is severely restricted by the level of its SOC, which must be more than 70 percent and cannot meet the maximum load demand.

3) SCENARIO (C): PV -WT WITH BESS

The third configuration turned on loads using RE (PV and WT) systems connected to a battery as an energy storage system. As shown in Figure 13, the number of turned-on loads increased compared with scenarios A and B because the electrical power generation increased when using a hybrid PV and WT with a battery as a backup system.

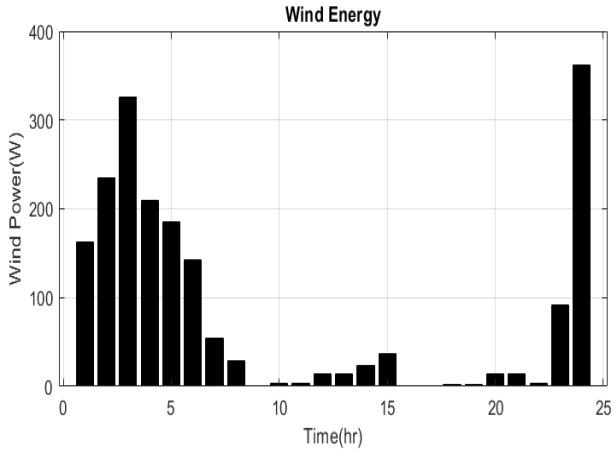

FIGURE 11. Wind power generation.

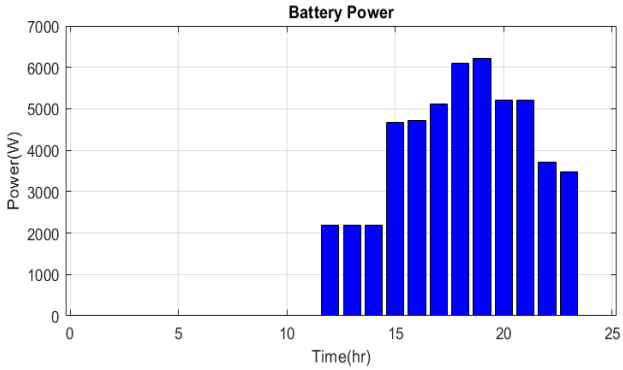

FIGURE 12. Backup battery power.

4) SCENARIO (D): PV-WT WITH BESS AND DG

As seen from the results of the previous scenarios, not all electrical loads were turned on. Therefore, to overcome the problem of prior scenarios, this configuration includes both RE (PV and WT) systems with BESS and DG to cover the remaining power consumption of loads. As shown in Figure 14, all the loads will be turned on, so it is a better configuration to be used in comparison with scenarios A, B, and C because the electrical power generation increases by using a Hybrid PV-WT with BESS and DG as a backup system.

B. ELECTRICAL POWER GENERATION UTILIZING GEOTHERMAL SYSTEM

This study deals with controlling the power generation from energy sources and calculating the cost of energy, which is simulated using the MATLAB program to operate the electrical loads for a home in Basrah City in the southern region of Iraq. Some values were assumed, as shown in Table 2, and were estimated previously using Equation (7). Then, the energy-saving value caused by the GS is calculated for one hour, assuming that the outside temperature is 44 °C. Then, the results for 15-23 hr. in which an air conditioner is needed can be calculated similarly.

Each Ton of Refrigeration (TR) equals 3.52 kW, so air conditioning with a capacity of 2 tons (2TR) will absorb heat; in contrast, it gives coolness with a value of ($2 \times 3.52 \cong 7kW$). In addition, each TR draws an electric current of approximately six amps, which means that approximately 1.5 kW of electric power implies that the air conditioner (2TR) draws an electrical energy of approximately 3 kW. The benefits of the GS, particularly the UHE, also known as the EAHE, are quantified by calculating the heat that the outside air removes when it passes through the UHE [66].

The inlet temperature, or ambient temperature, of Iraq is assumed to be $T_i = 44$ °C, and after passing through the UHE, the temperature drops to 34°C. The temperature of the soil was measured at a depth of 5m, $T\ (z, t) = 27$°C. Once the soil temperature and heat transfer coefficient were determined using the assumed values, the saved energy and cooling savings were calculated, as shown in Figure 16. In this study, we used a cooling load (an air conditioner) of 2500 W for 9 hr. This means that only a large amount of power is consumed for this load. To decrease the power consumption value for this load, we use a GS, EAHE, which will affect the air conditioner by decreasing its power consumption, as shown in Figure 15. This leads to savings in electrical power due to temperature reduction in the UHE, which is calculated using Equation (13). The coefficient of performance is calculated mathematically, as shown in Equation (15), which is the ratio between the cooling rate and electrical power consumption. Whenever a higher coefficient of performance means that less power consumption is required for the same output, it lowers the operating costs.

$$Coefficient\ of\ Performance = \frac{Cooling\ rate}{Electrical\ consumption} \tag{15}$$

A comparison between Figures 7 and 15 reveals that at a point located at X19, which refers to the daily load profile at the time of operation, power consumption of the air conditioner decreases from 6125 to 5501W by adding a GS. This leads to a reduction in electrical power. After utilizing a GS, the battery and DG power generation are changed because of the decreased total load power. The previous calculations were performed for the assumed temperature. Figure 16 shows the GS parameter calculations for the inlet and outlet air temperature, energy saving percentage, soil temperature, saved energy, and load curve with and without GS.

Figure 16 shows the calculation result of GS parameters, such as soil temperature, which is between 27°C and 28°C, and according to its value, the inlet temperature that enters the room is calculated. Compared with the outlet temperature, its value decreases, as shown in the air temperature curve, and the percentage of energy saving curves shows the values needed to calculate the saved energy values, which are clarified in the curve of saved energy. The load curves are changed before and after using a GS; before using a GS at a time between 15 and 23 hr., the load curve is greater than

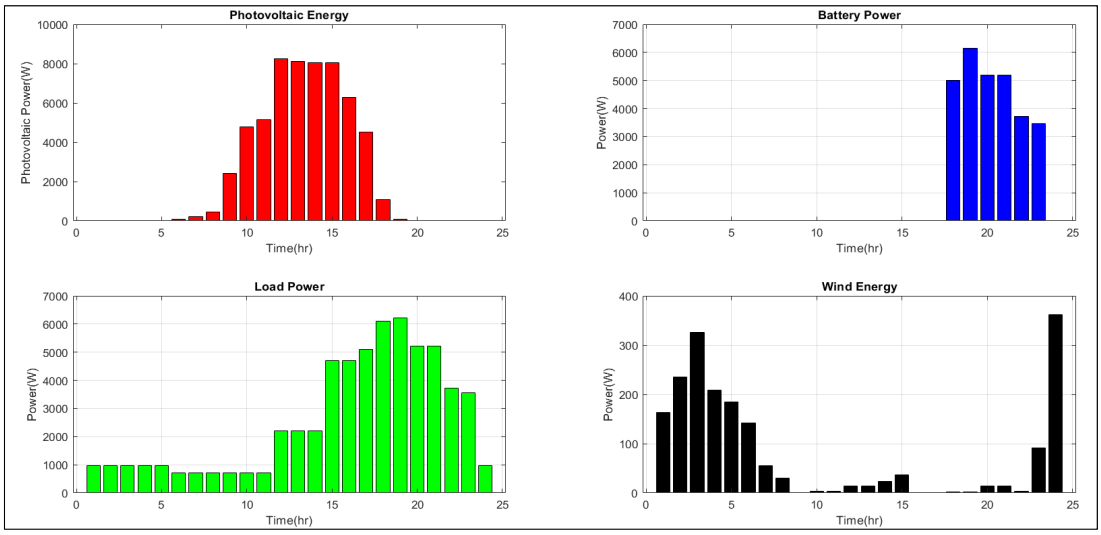

FIGURE 13. PV-WT-battery power generation.

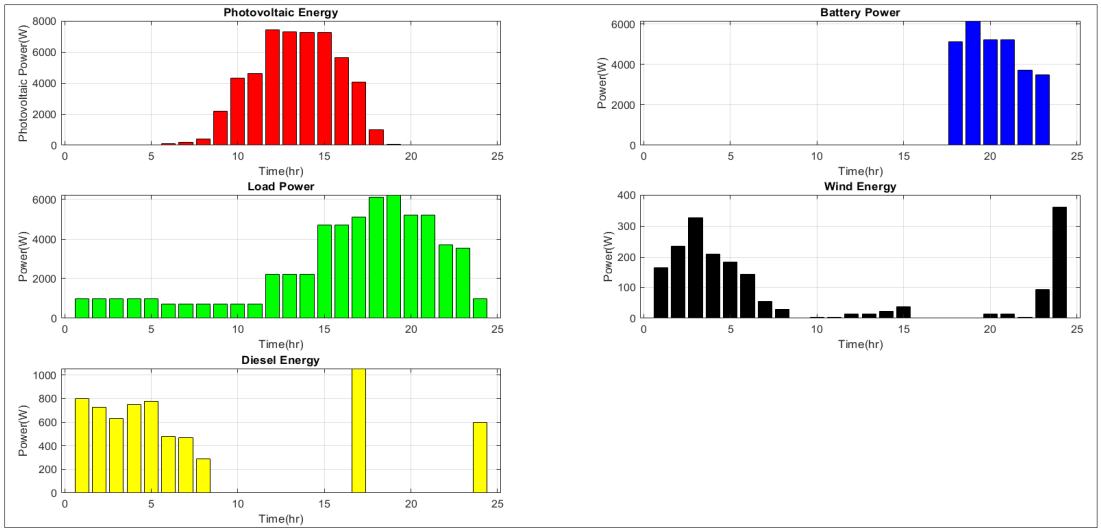

FIGURE 14. HS with battery and DG system power generation.

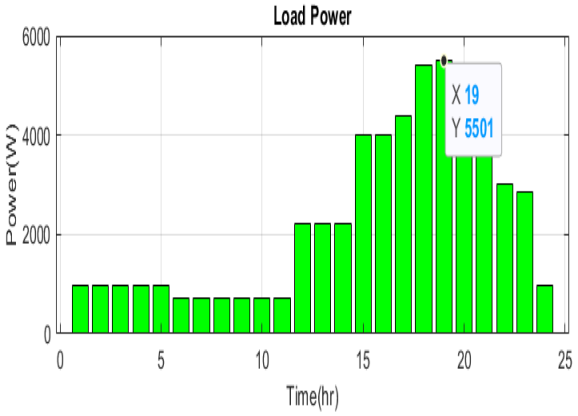

FIGURE 15. Hourly load power over one day utilizing a GS.

the other one; however, when using a GS, it is calculated depending on the change in the inlet temperature relative to the outlet temperature, which leads to calculation of the saved energy and the percentage of savings, which affects the air conditioner power and decreases its value.

Therefore, the load curve shows a reduction in power when the air condition was turned on, as shown in the load curves with and without the GS. This study simulated two scenarios for PV-WT-BESS with GS; the other scenario, using PV-WT-BESS and DG with GS is discussed below.

1) SCENARIO(A): PV-WT WITH BESS UTILIZING GS

In this scenario, the battery power values decreased after GS was utilized. This change was due to a reduction in the total load power resulting from the use of a GS with a UHE. This reduces the temperature of the atmosphere to a lesser degree than inside the room, thus allowing for the calculation of energy savings that affects the electrical power consumption of the air conditioner load. Consequently, power

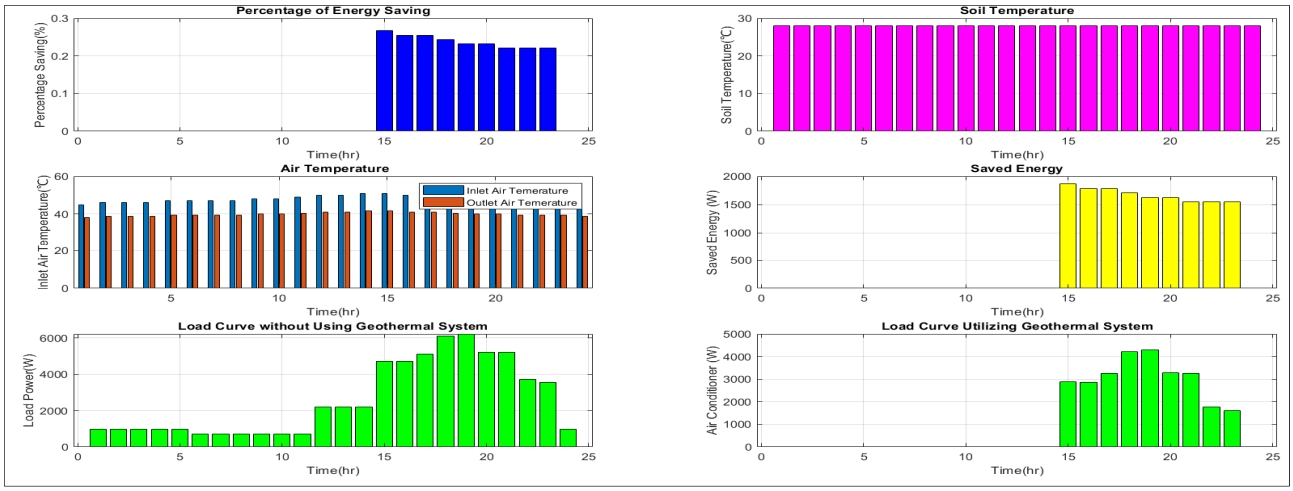

FIGURE 16. GS parameters calculation and load curve with and without using a GS.

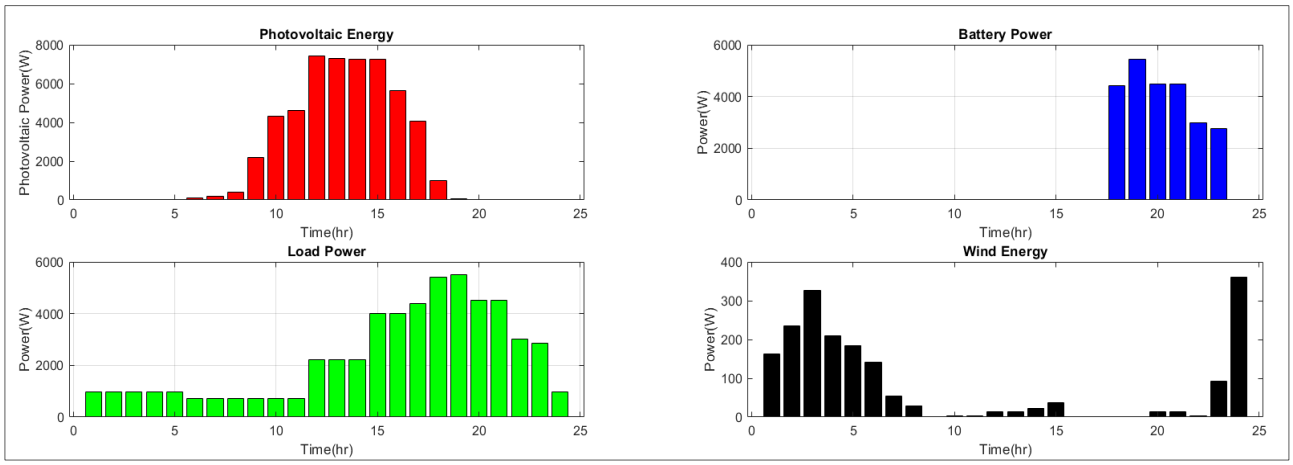

FIGURE 17. PV-WT-battery power generation with GS.

generation decreases according to this reduction, as shown in Figure 17.

Compared to Figures 13 and 17, the power demand starts decreasing between 15 and 23 hr., the period related to the air conditioner being turned on. Because its power is declining, this leads to a decrease in the energy drawn from the battery owing to the reduction in power demand during those hours, benefiting from using a GS.

2) SCENARIO (B): PV-WT WITH BESS AND DG UTILIZING GS

As shown in Figure 18, the DG power generation will decrease when operating the air conditioner due to a decrease in the total power demand caused by the impact of using a GS.

As shown in Figure 14, all loads are turned on using a (PV-WT) with BESS and DG without the addition of a GS, where the power drawn from the DG and batteries that are needed to turn on all loads is greater than the power generated, as shown in Figure 18, where GS helps reduce the load consumption of the air conditioner.

V. ECONOMIC EVALUATION OF THE RESULTS

Although PV and WT are accessible and inexpensive fuel energy sources, they suffer from the cost of capital depreciation. In this section, we present the results of these costs. The mathematical cost equation of this study includes the costs of the PV, WT, BESS, DG, and GS, as shown below:

$$\begin{aligned} &C_{Source} \\ &= C\,(renewable, diesel, bat., geothermal) \\ &= \left(C_{pv} \times P_{pv} + C_{wt} \times P_{wt} + C_{DG} \times P_{DG} + C_{bat} \times P_{bat} + C_{gth}\right) \end{aligned} \tag{16}$$

where C_{Source} is the source power cost, C_{pv} is the PV system cost, P_{pv} is the PV power , C_{wt} is the WT system cost, P_{wt} is the WT power, C_{DG} is the DG cost, P_{DG} is the DG power,

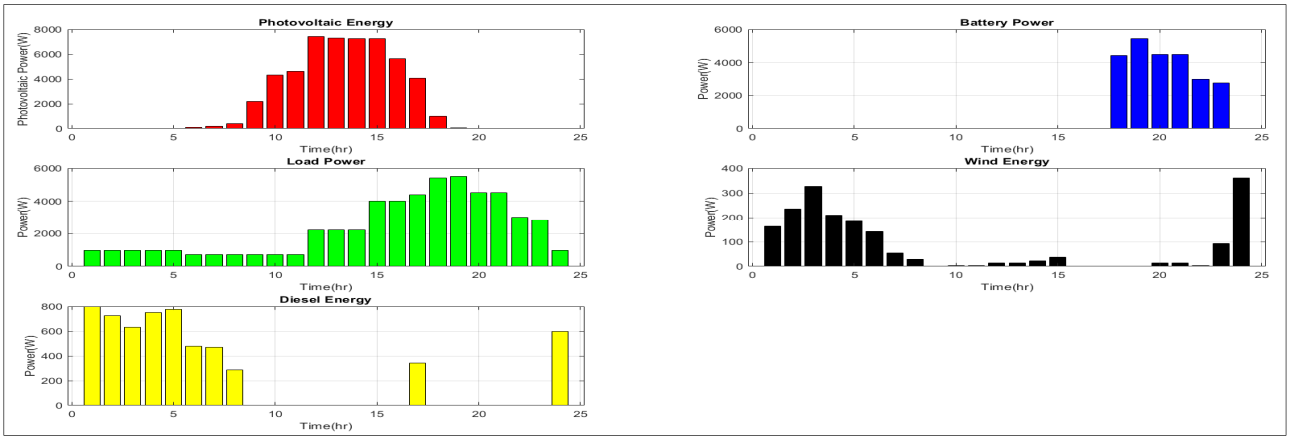

FIGURE 18. PV-WT-battery-DG power generation utilizing GS.

C_{bat} is the BESS cost, P_{bat} is the battery power and C_{gth} is the GS operating cost.

A. MATHEMATICAL MODEL OF PHOTOVOLTAIC ENERGY COST

The total cost of a PV power system ($/kW) was calculated as [63].

$$C_s = \frac{IC_s}{Y_{proj} \times E_s} + \frac{M_{year}}{E_s} \tag{17}$$

where C_s is the total cost of PV power, IC_s is the initial cost of PV power, which is a function of the placement and design of the solar arrays and is calculated using Equation (18), M_{year} is the annual maintenance and cleaning cost for solar panels, Y_{proj} is the project lifetime, E_s is the total PV energy per year (E_s = PV power $\times$ time).

$$IC_s = N_s \times C_{sc} \times \left(\frac{i \times (1+i)^{Y_{proj}}}{(i+1)^{Y_{proj}} - 1} \right) \tag{18}$$

where IC_s is the initial cost of PV power, N_s is the number of solar arrays, C_{sc} is the capital cost of the solar panel plus the cost of installation, i is the real interest rate, which is required to be 5%, and Y_{proj} is the project lifetime [63].

B. MATHEMATICAL MODEL OF WIND ENERGY COST

The cost of WT ($\boldsymbol{C_{wind}}$) is calculated as [55]:

$$C_{wind}(t) = (C_{capital,wind} + \frac{Com_{wind}}{8760}) \tag{19}$$

where $C_{wind}(t)$ is the total cost of WT power, $C_{capital,wind}$ is the capital cost of WT, which is calculated using Equation (20), Com_{wind} represents the operation and maintenance cost of WT [55].

$$C_{capital,wind} = \frac{IC_w \times \frac{i(1+i)^{Y_{proj}}}{(1+i)^{Y_{proj}}-1}}{P_{wind,rated} \times CF_{wt} \times 8760} \times P_{wt} \times t \tag{20}$$

where $C_{capital,wind}$ is the capital cost of the WT, IC_w is the initial cost of the WT, i is the interest rate, Y_{proj} is the project's lifetime, $P_{wind,rated}$ rated power of WT, CF_{wt} is the WT capacity factor [63]. The initial cost was calculated using Equation (21).

$$IC_w = \left(0.1 \times \left[\frac{h}{10} - 1\right] + 1\right) \times N_w \times \left(2.449 \times r^{2.7} + C_{wf}\right) \times \left(\frac{i \times (1+i)^{Y_{proj}}}{(i+1)^{Y_{proj}} - 1} \right) \tag{21}$$

where IC_w is the initial cost of the WT power, h is the height of the wind tower, N_w is the number of WTs, r is the WT radius, C_{wf} is the installation and fabrication cost of the WT, i is the real interest rate, and Y_{proj} is the project lifetime [63].

C. MATHEMATICAL MODEL OF BATTERY COST

HS require energy storage devices to manage and control generation variations. Batteries are the most essential components of HS. Battery cost C_{bat} is calculated as follows:

$$C_{bat} = C_{wc,bat} \times |P_{bat}| \times t + C_{O\&M,bat} / 8760 \tag{22}$$

where C_{bat} is the battery cost, $C_{wc,bat}$ is the battery wear cost, which is calculated using Equation (23), P_{bat} is the battery power in each hour, t is the time, $C_{O\&M,bat}$ is the operation and maintenance costs of the battery.

$$C_{wc,bat} = \frac{C_{rep,bat}}{N_{bat} \times Q_{lifetim} \times \sqrt{\eta_{bat}}} \tag{23}$$

where $C_{wc,bat}$ is the battery wear cost, $C_{rep,bat}$ is the battery replacement cost, N_{bat} is the number of batteries, $Q_{lifetim}$ is the battery lifetime, and η_{bat} is the battery efficiency [55].

D. MATHEMATICAL MODEL OF DIESEL GENERATOR COST

The fuel consumption of the DG unit is related to the rated and generated powers. The cost of fuel consumption can be calculated hourly, as follows [64]:

$$HFC = C_f \times \sum_{t=1}^{Tend} D_f(t) \tag{24}$$

where HFC is the hourly fuel cost of DG, C_f is the fuel cost per liter, $D_f(t)$ is the consumption of fuel per hour. $D_f(t)$ can

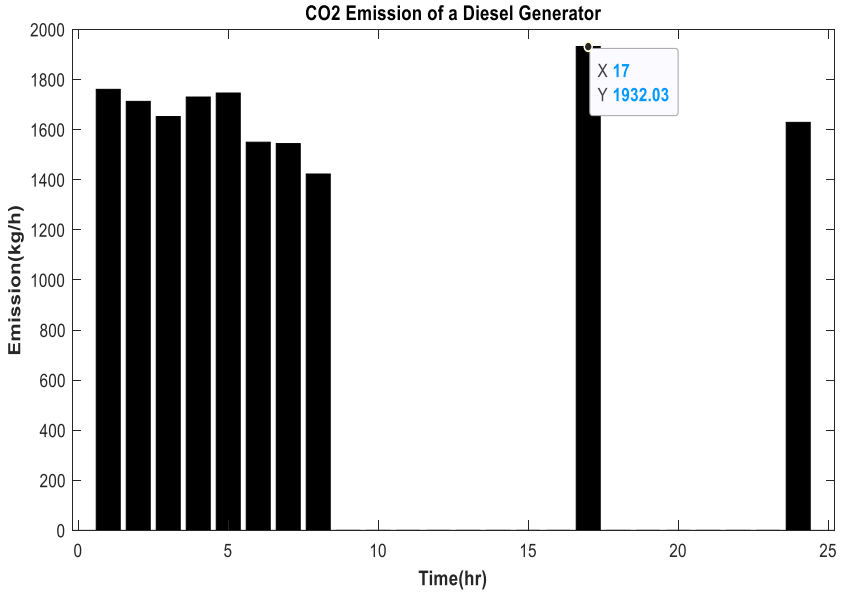

FIGURE 19. CO_2 Emission of DG without utilizing GS.

be calculated using Equation (25) [64].

$$D_f\,(t) = (0.246 \times P_{DG}\,(t) + 0.08415 \times P_{DGr}) \tag{25}$$

where $D_f\,(t)$ is the hourly fuel consumption of the DG in *liter/hr.*, P_{DG} is the DG average power per hour in *kW*, P_{DGr} is the rated power of a DG in *kW*, α_D and β_D are the fuel consumption curve coefficients in *liter/kWh* [61].

E. MATHEMATICAL MODEL OF GEOTHERMAL SYSTEM COST

The mathematical model for the GS cost depends on some factors and can be calculated as follows [65]:

$$C_{geothermal,year} = \frac{C_{pipe} + C_{dr\&cr}}{Y_{proj}} + C_m \tag{26}$$

where $C_{geothermal,year}$ is the yearly cost of a GS, C_{pipe} is the pipes cost, $C_{dr\&cr}$ is the cost of drilling and creation, C_m is the maintenance cost and Y_{proj} is the project lifetime. It appears that there is no need for a large amount of maintenance; therefore, maintenance costs are minimal.

In this study, we manage the energy consumption of loads and electrical power generation sources and evaluate the results from an economic perspective. Therefore, we calculated the cost per hour for all equipment in the HS, assessed the total cost for the scenario with and without utilizing the GS, and compared them. The total cost of this study canb e calculated using Equation (16). The values of the parameters assumed in Table 2 were used to calculate the cost equation for the PV, WT, BESS, and DG with and without the GS.

Using the previously mentioned equations, we can calculate the total cost imposed on the system in each scenario. Equation (16) calculates the cost per hour. However, our model manages the load and generation every 15 min to evaluate the hourly cost economically.

F. COMPARING THE SCENARIOS FROM EMISSION VIEW POINT AND THE ECONOMIC ASPECTS

1) EMISSION VIEWPOINT

DG emits greenhouse gases such as carbon dioxide (CO_2). However, because of the conditions within the combustion chamber and the time required for mixing air and fuel, hydrocarbon fuel is not entirely burned, leading to carbon monoxide. It is essential to recognize that at high temperatures, CO_2 initiates dissociation into CO, and the incomplete combustion of fuel results in the presence of hydrocarbons in the emissions. The fuel consumption is directly correlated with the release of CO_2 into the atmosphere. The emission of CO_2 increases with increasing fuel consumption [70].

DG is a conventional energy source used as a backup system to supply power in combination with an HRES. The hourly fuel consumption of DG was calculated using Equation (6).

We chose to measure pollutant emissions in kilograms of CO_2 because of their significant contribution to the greenhouse effect and their high percentage among all emissions resulting from fuel combustion [69]. To do this, we calculated the value of CO_2 emissions as follows [7]:

$$E_{CO_2}\,(\mathrm{t}) = S_{E(CO_2)} \times D_f\,(t) \tag{27}$$

where $E_{CO_2}\,(\mathrm{t})$ is the value of CO_2 emissions in *kg/hr.*, $S_{E(CO_2)}$ is the CO_2 specific emission per liter of fuel in *kg/l* which is given by (2.7), and $D_f\,(t)$ is the consumption of fuel per hour in *liter/hr.* [7].

a: SCENARIO: (A): CO_2 EMISSION OF DG WITHOUT UTILIZING GS

Figure 19 shows the CO_2 emissions of a DG without utilizing a GS.

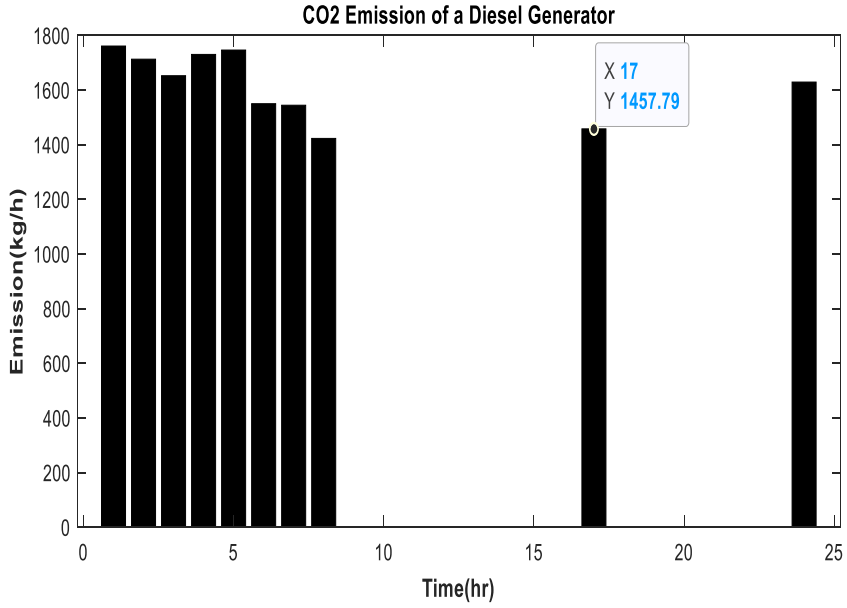

FIGURE 20. CO_2 Emission of DG utilizing GS.

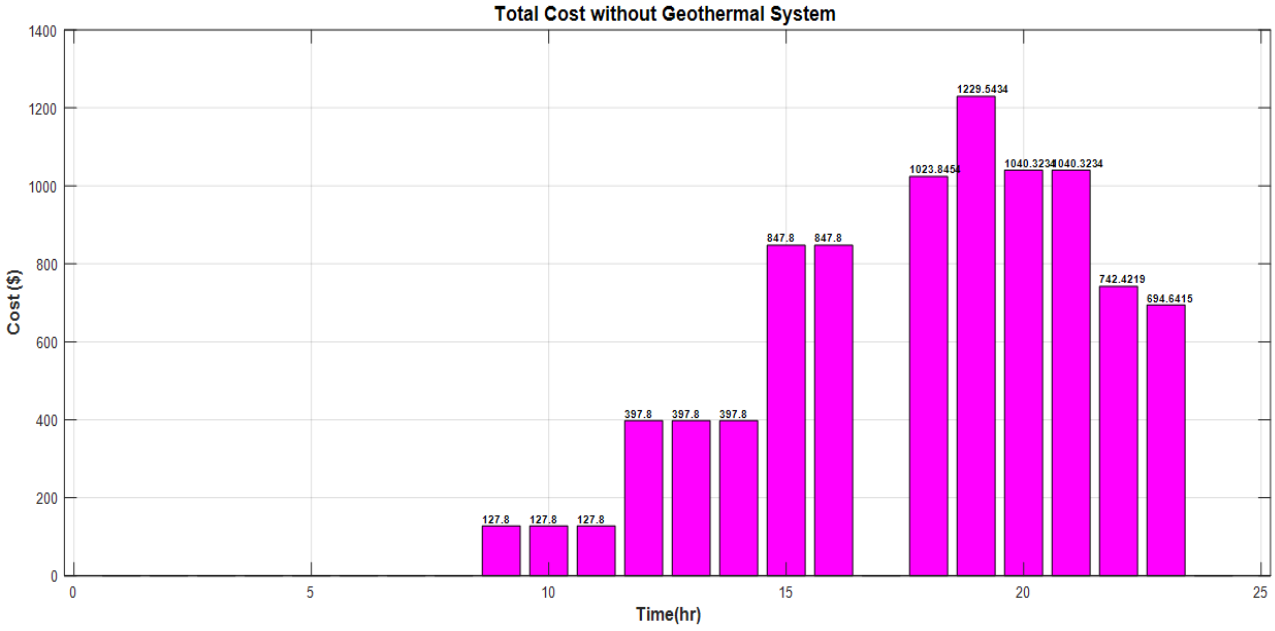

FIGURE 21. The total cost of PV-WT-BESS without utilizing GS.

b: SCENARIO (B): CO_2 EMISSION OF DG UTILIZING GS

Figure 20 shows the CO_2 emission of a DG utilizing a GS.

As shown in Figures 19 and 20, the difference between these figures is shown as a numeral of X17, which indicates the time needed to operate DG when the energy power from the (PV-WT-battery) energy source is insufficient. At this time, we need to cover the total power demand by adding DG as a backup source, so Figure 19 shows that the CO_2 emission of a DG at time 17 is calculated as 1932.03. Figure 20 shows that the value calculated for the CO_2 emissions of the DG at time 17 decreased to 1457.79. This reduction is due to the utilization of a GS, which reduces the demand for air conditioner power, leading to a decrease in the power drawn from the DG, and consequently reducing the value of diesel fuel consumption. The CO_2 emissions also decreased.

2) THE ECONOMIC ASPECTS

In this section, two scenarios are simulated for the PV-WT-BESS without GS, and the other scenario using PV-WT-BESS and DG without GS is discussed below.

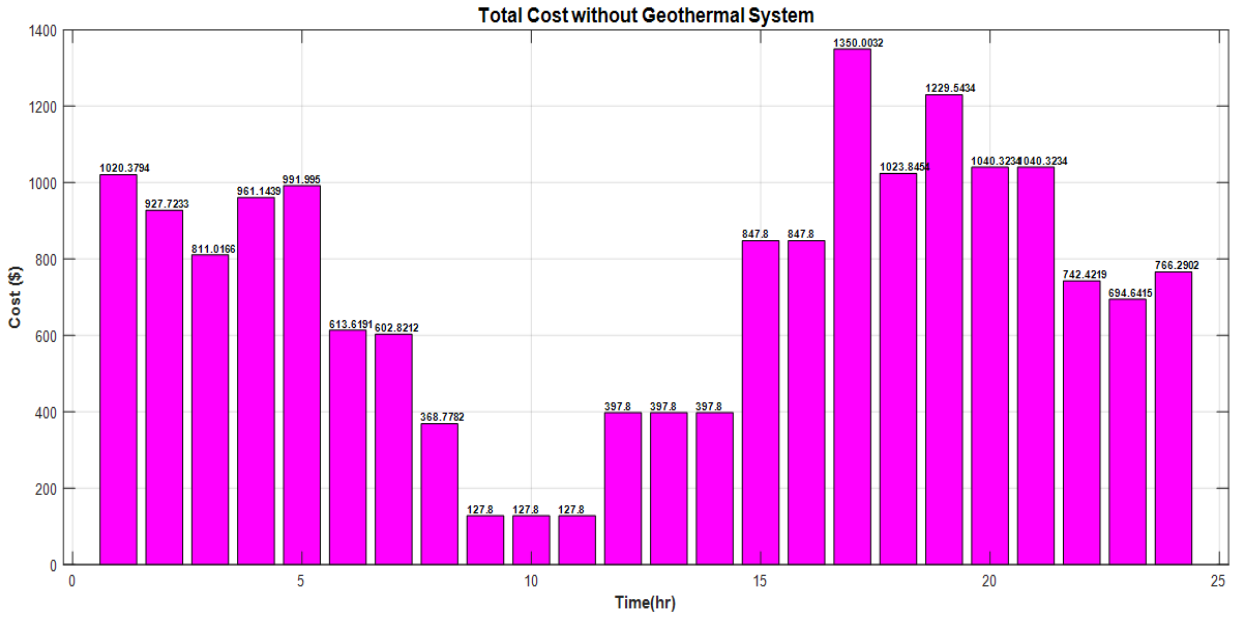

FIGURE 22. The total cost of PV-WT-BESS-DG without utilizing GS.

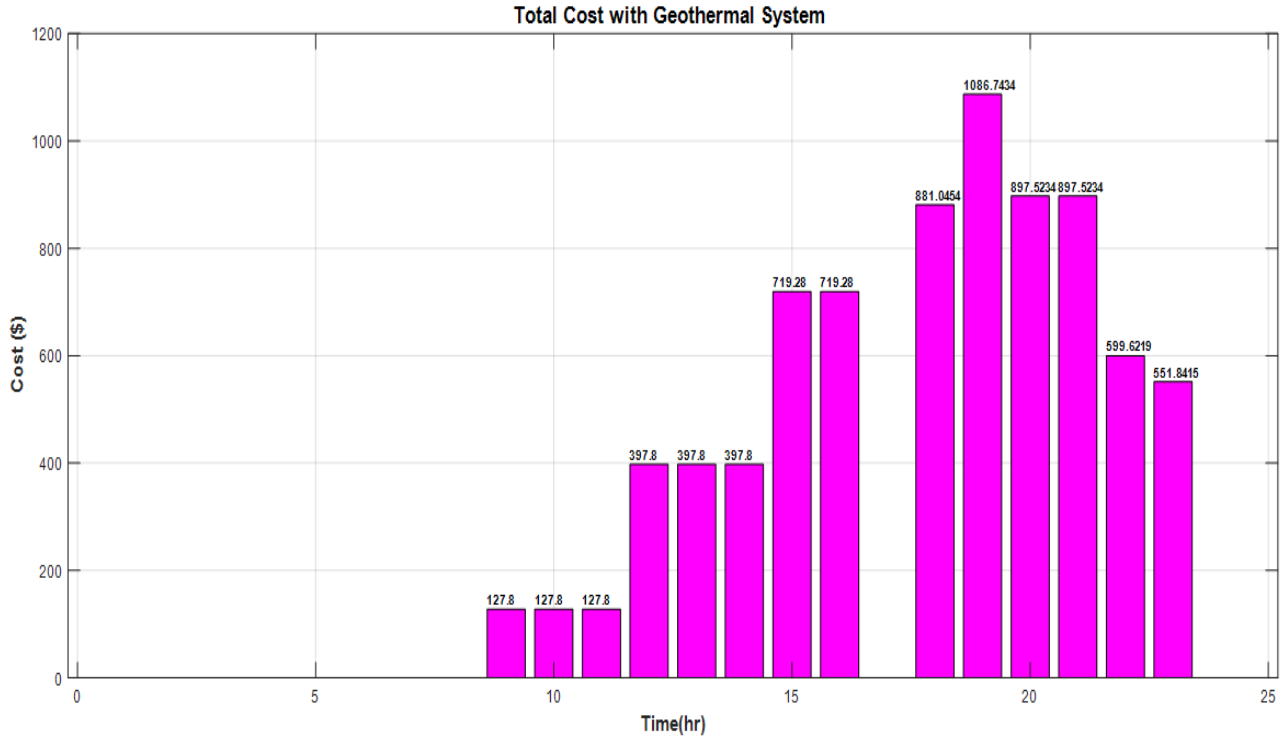

FIGURE 23. The total cost of PV-WT-BESS utilizing GS.

a: SCENARIO: (A) PV-WT-BESS WITHOUT UTILIZING GS

Figure 21 shows the total cost of the proposed system (PV-WT-BESS) without GS.

b: SCENARIO (B): PV-WT-BESS-DG WITHOUT UTILIZING GS

Figure 22 shows the total cost of the proposed system (PV-WT-BESS-DG) without GS.

3) ECONOMICAL EVALUATION OF THE RESULTS UTILIZING A GEOTHERMAL SYSTEM

In this section, two scenarios are simulated for the PV-WT-BESS utilizing GS and the other scenario using the PV-WT-BESS and DG utilizing GS, as explained below:

According to Equation (26), the calculation of the GS cost depends only on the initial cost.

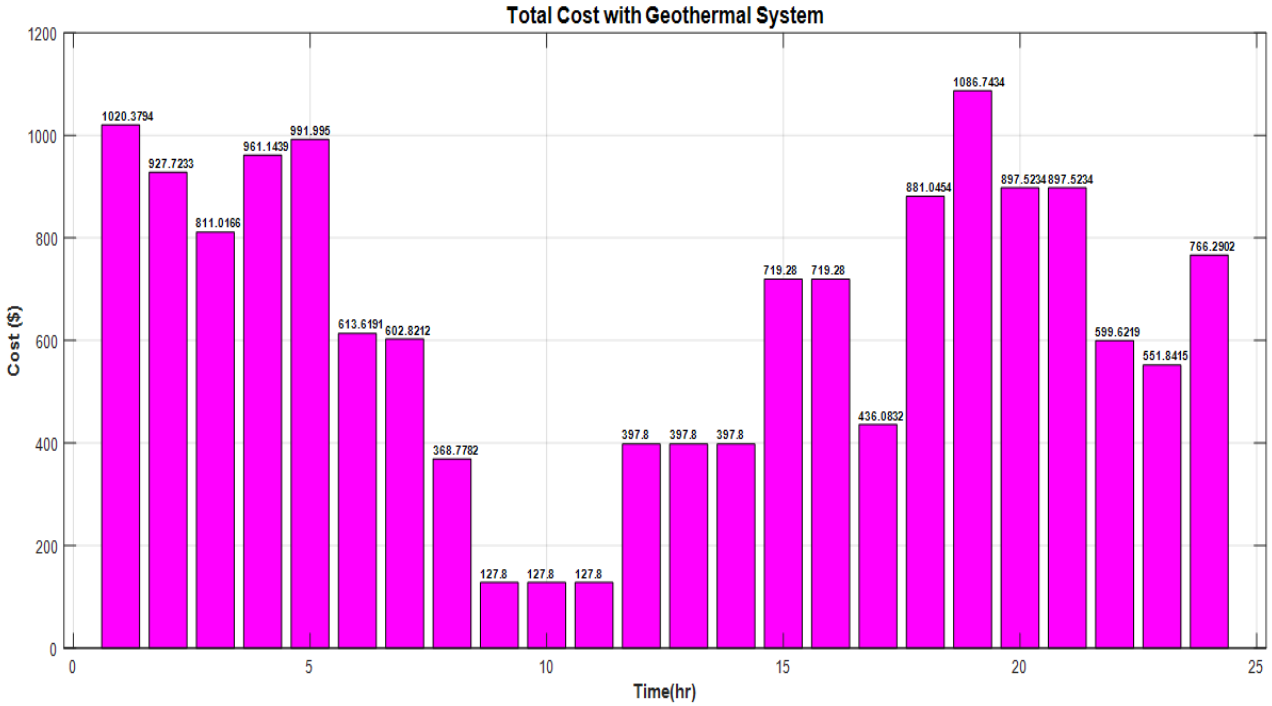

FIGURE 24. The total cost of PV-WT-BESS-DG utilizing GS.

FIGURE 25. Hourly load power over one day.

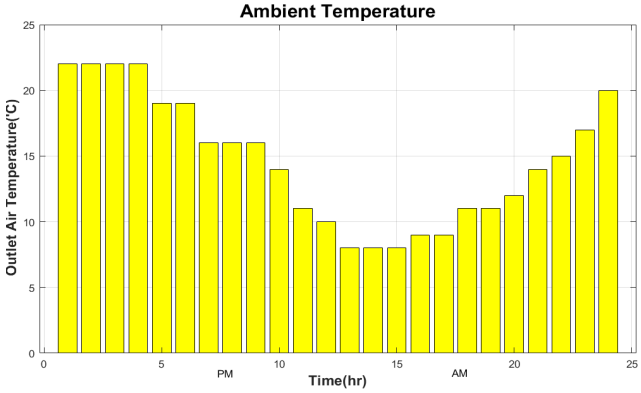

FIGURE 26. Hourly ambient temperature for Jan. 25 in Basrah Ira.

Supposing the following parameters (that are close to reality):

$$C_{pipe} = 75\$,\ C_{dr\&cr} = 150\$,$$
$$C_m = \frac{10\$}{year},\ Y_{year} = 30\ \text{yr}.$$

Then: $C_{geothermal,year} = \frac{C_{pipe}+C_{dr\&cr}}{Y_{year}} + C_m$

$$\text{GS (cost/year)} = \frac{75+150}{30} + 10 = 17.5\$/\text{year}$$

This cost is lower than the energy savings. Moreover, there is no need for a large amount of maintenance; therefore, the maintenance costs are minimal.

a: SCENARIO (A): PV-WT-BESS UTILIZING GS

The result of MATLAB programming for the total cost calculation shown in Figure 23 reveals that the total cost is reduced after using the GS, which affects the power consumption of the air conditioner load, leading to a reduction in the power drawn from the battery, which causes a decrease in the cost value.

b: SCENARIO (B): PV-WT-BESS-DG UTILIZING GS

In this scenario, the total cost calculation results obtained using all electrical power energy sources are shown in Figure 24. This figure shows that the total cost is reduced by using GS, which decreases the power consumption of the air conditioner load. This leads to a reduction in the power drawn from the battery, which causes a decrease in cost.

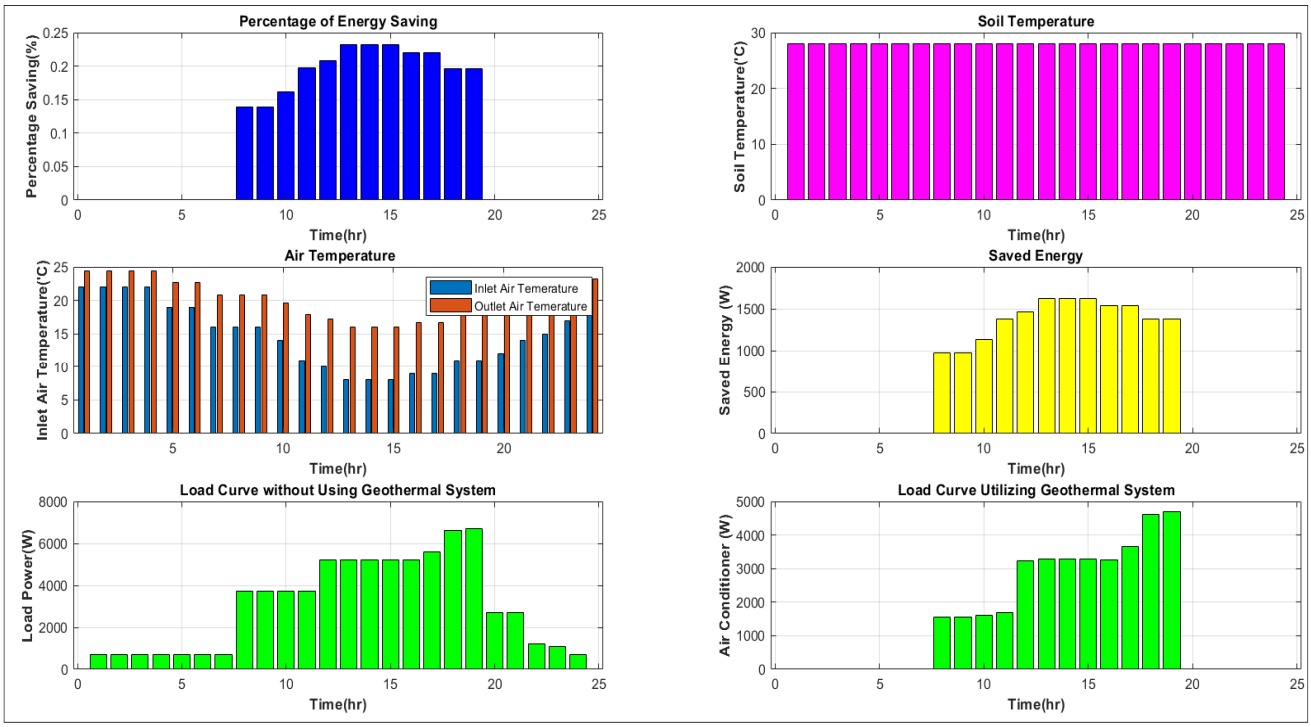

FIGURE 27. GS parameters calculation and load curve with and without using a GS in winter.

Comparing Figures 21 and 23, and Figures 22 and 24, it is evident that the total cost decreases when the air conditioner is turned on between 15 and 23 hr. It is clear that when utilizing a GS, the power consumption of the air conditioner decreases. Compared to the case of not using a GS, this leads to a reduction in the cost of generating power sources and power savings.

G. COMPARING THE SCENARIOS FROM EMISSION VIEW POINT AND THE ECONOMIC ASPECTS FOR THE WINTER SEASON

Suppose that we have the same load profile used for the summer season, replacing the air cooler and air conditioner loads with a new load (electrical heating load with a power of 3kW for winter) and an operation time between 8 PM and 19 AM. The latest load profile is shown in Figure 25.

Figure 26 shows the hourly ambient temperature measured in Basrah, Iraq, over one day in January.

Figure 27 shows the GS parameter calculations for the inlet and outlet air temperature, energy saving percentage, soil temperature, saved energy, and load curve with and without GS in winter.

Figure 27 shows the calculation result of the GS parameters, such as soil temperature, which is between 27°C and 28°C, and according to its value, the inlet temperature that enters the room is calculated. Compared with the outlet temperature, its value increased, as shown in the Air Temperature curve, where the inlet temperature degrees were lower than the outlet temperature degrees that entered the home. The Percentage of Energy Saving curve shows the values needed to calculate the Saved Energy values, which are clarified in the curve of Saved Energy. The load curves are changed before and after using a GS; before using a GS at a time between 8 PM – 19 AM, the load curve is greater than the other one; however, when using a GS, it is calculated depending on the change in the inlet temperature relative to the outlet temperature, which leads to calculating the saved energy and the percentage of savings, which affects the electrical heating power and decreases its value. Therefore, the load curve shows decrease in power at those hours when the electrical heating is turned on, as shown in the curve of load with and without utilizing the GS. In this study, the two scenarios were simulated regarding emission viewpoint and economic aspects in the winter season for PV-WT-BESS with and without GS; the other scenario using PV-WT-BESS and DG with and without GS is discussed below:

1) EMISSION VIEWPOINT

As discussed in Section V-F1, to calculate the emissions during the summer season, the same procedure was used for the winter season, considering the changing load profile and ambient temperature.

a: SCENARIO: (A): CO_2 EMISSION OF DG WITHOUT UTILIZING GS

Figure 28 shows the CO_2 emissions of DG without GS during the winter season.

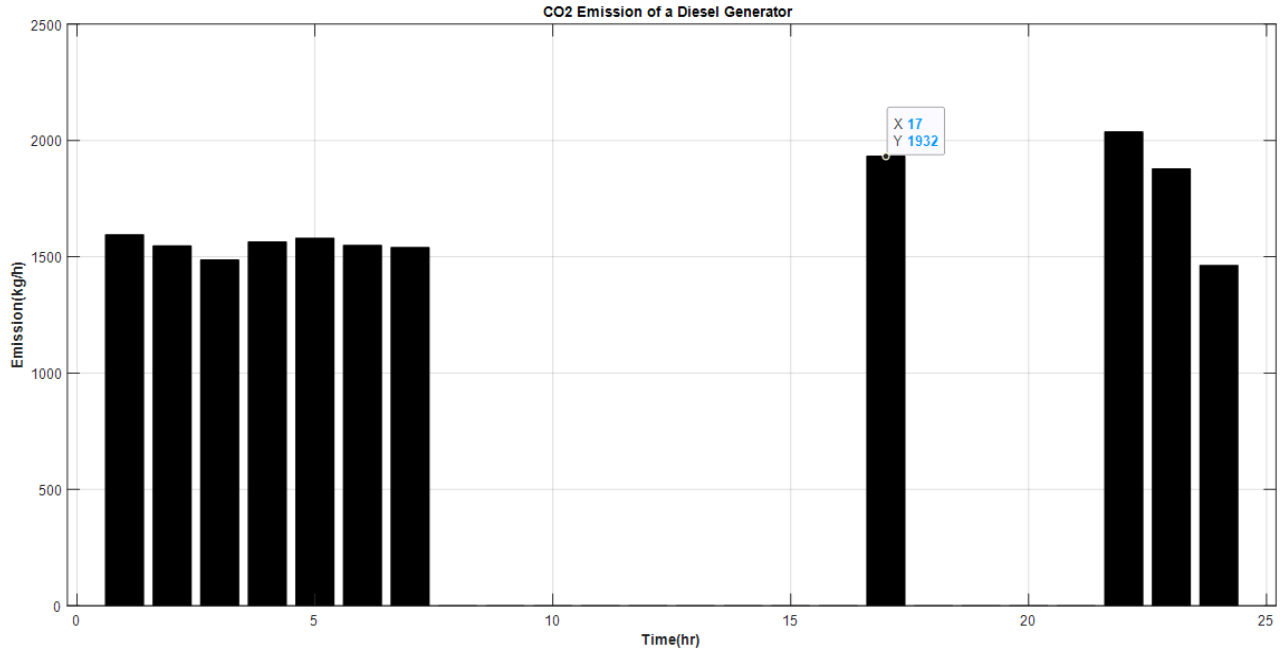

FIGURE 28. CO_2 Emission of DG without utilizing GS in winter season.

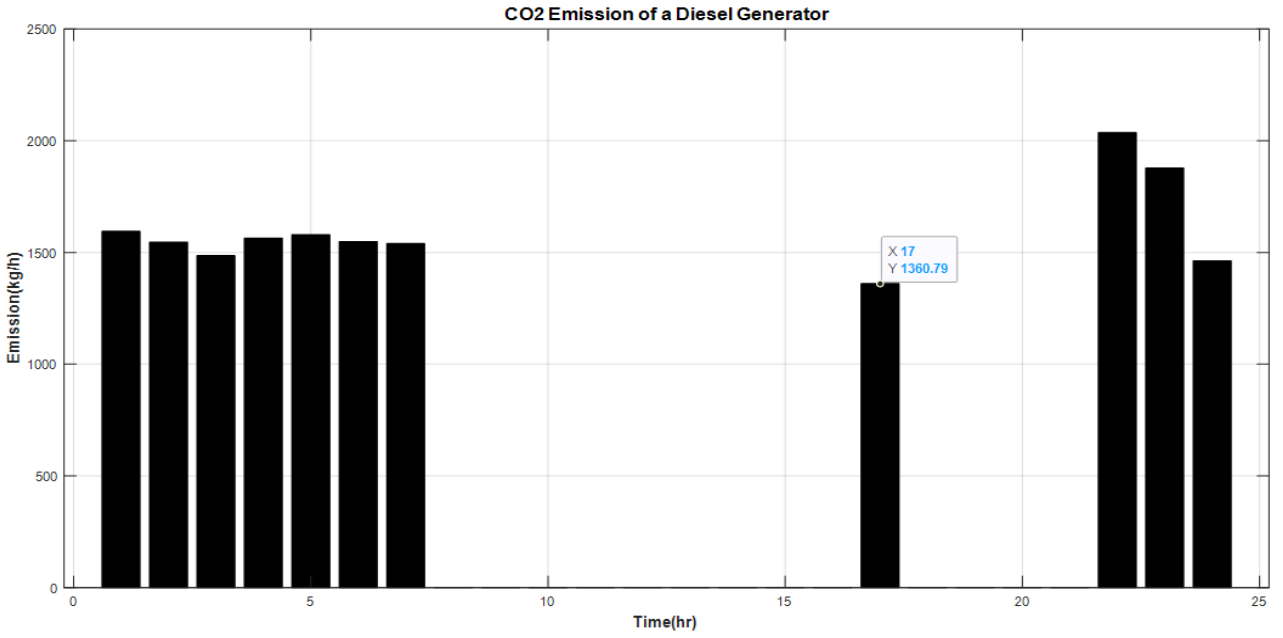

FIGURE 29. CO_2 Emission of DG utilizing GS in winter season.

b: SCENARIO (B): CO_2 EMISSION OF DG UTILIZING GS

Figure 29 shows the CO_2 emissions of the DG utilizing a GS during the winter.

As shown in Figures 28 and 29, the difference between these figures is shown as a numeral of X17, which indicates the time needed to operate the DG when the energy power from the (PV-WT-battery) source is insufficient. At this time the total power demand needs to be cover by adding DG as a backup source; thus, Figure 28 shows that the CO_2 emission of DG at time 17 was calculated as 1932. Figure 29 shows that the value calculated for the CO_2 emissions of DG at time 17 decreased to 1360.79. This reduction is due to the utilization of a GS, which reduces the demand for electrical heating power, diminishing the power drawn from the DG and consequently decreasing the diesel fuel consumption. The CO_2 emissions were also reduced.

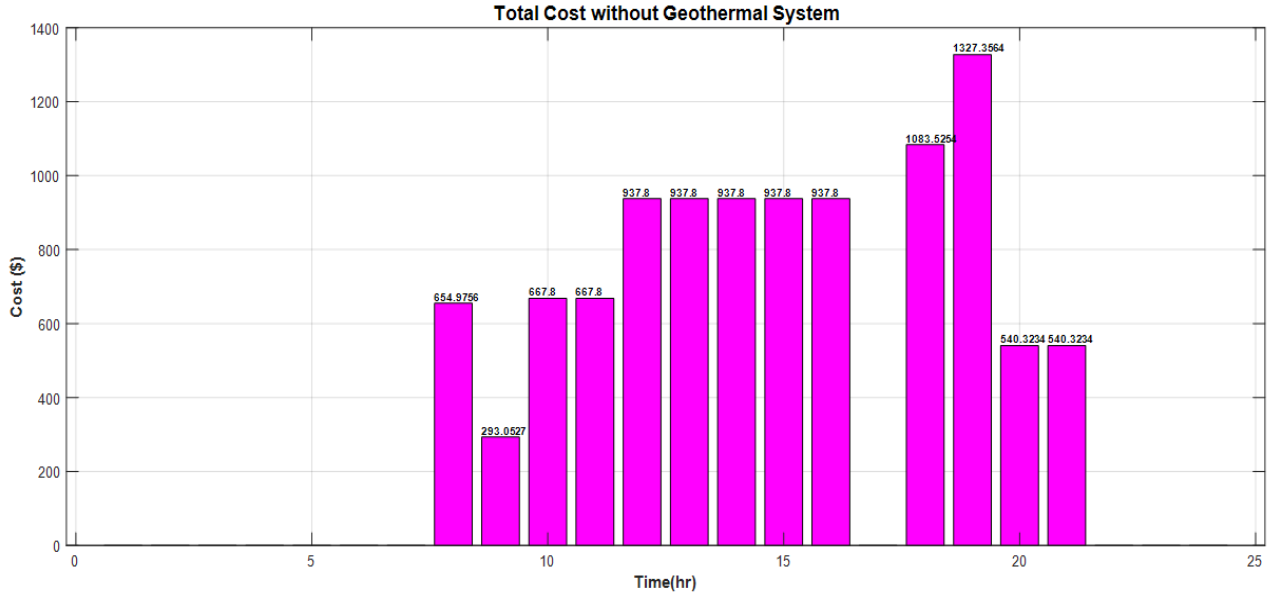

FIGURE 30. The total cost of PV-WT-BESS without utilizing GS in winter season.

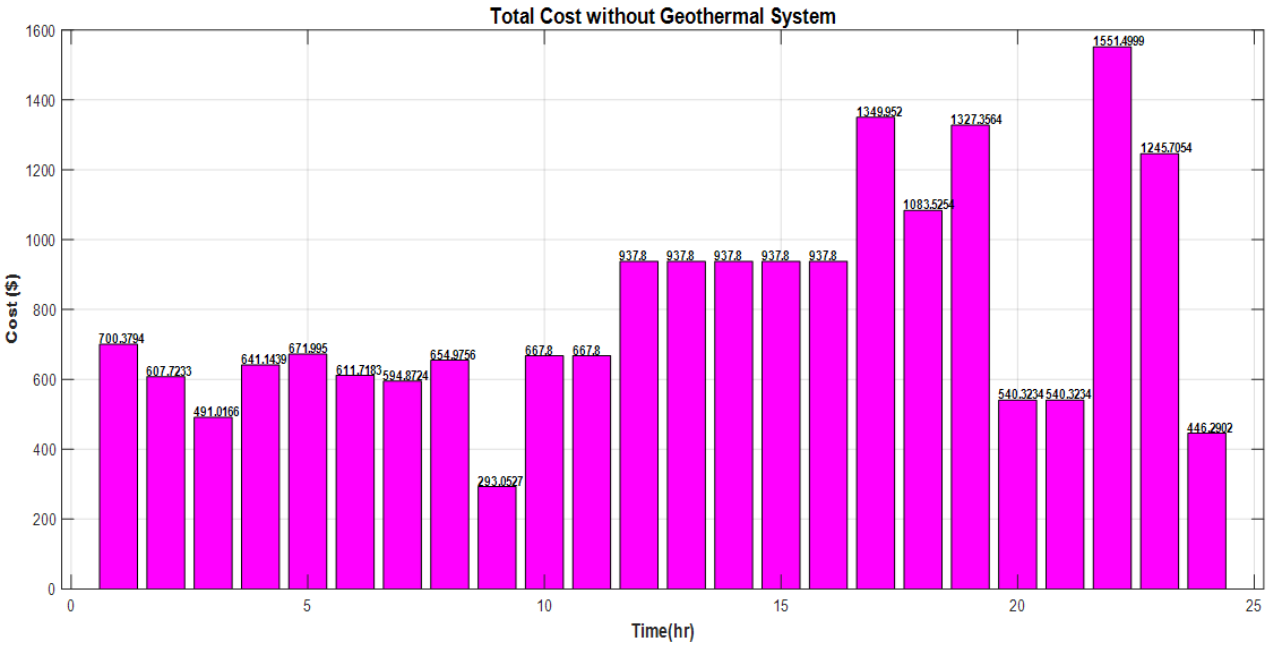

FIGURE 31. The total cost of PV-WT-BESS-DG without utilizing GS in winter season.

2) THE ECONOMIC ASPECTS

In this section, two scenarios to calculate the total cost for the winter season are simulated for PV-WT-BESS without GS, and the other scenario uses PV-WT-BESS and DG without GS, as discussed below.

a: SCENARIO: (A) PV-WT-BESS WITHOUT UTILIZING GS

Figure 30 shows the total cost of the proposed system (PV-WT-BESS) without a GS during the winter season.

b: SCENARIO (B): PV-WT-BESS-DG WITHOUT UTILIZING GS

Figure 31 shows the total cost of the proposed system (PV-WT-BESS-DG) without a GS during the winter season.

3) ECONOMICAL EVALUATION OF THE RESULTS UTILIZING A GEOTHERMAL SYSTEM(GS)

In this section, two scenarios for calculating the total cost in the winter season are simulated for PV-WT-BESS utilizing

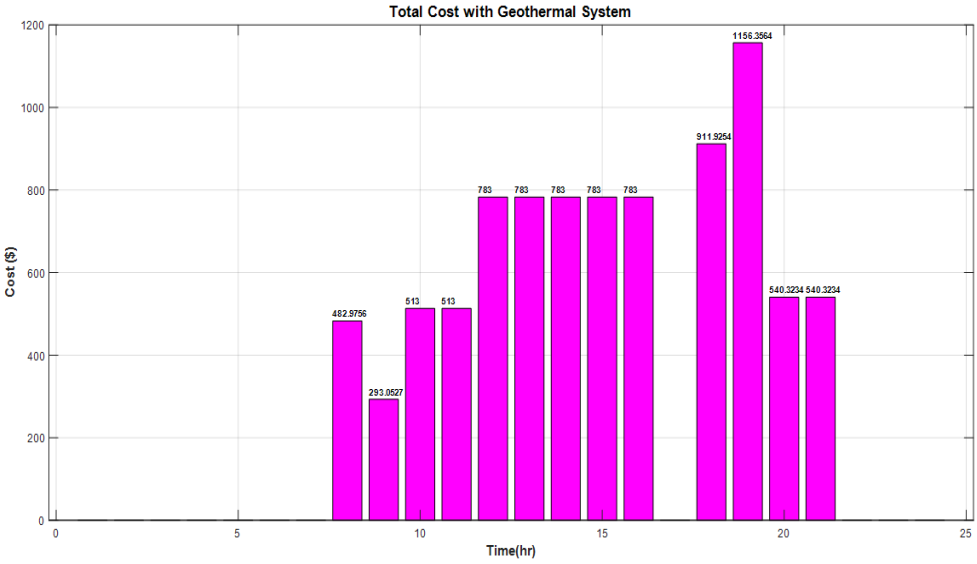

FIGURE 32. The total cost of PV-WT-BESS utilizing GS in winter season.

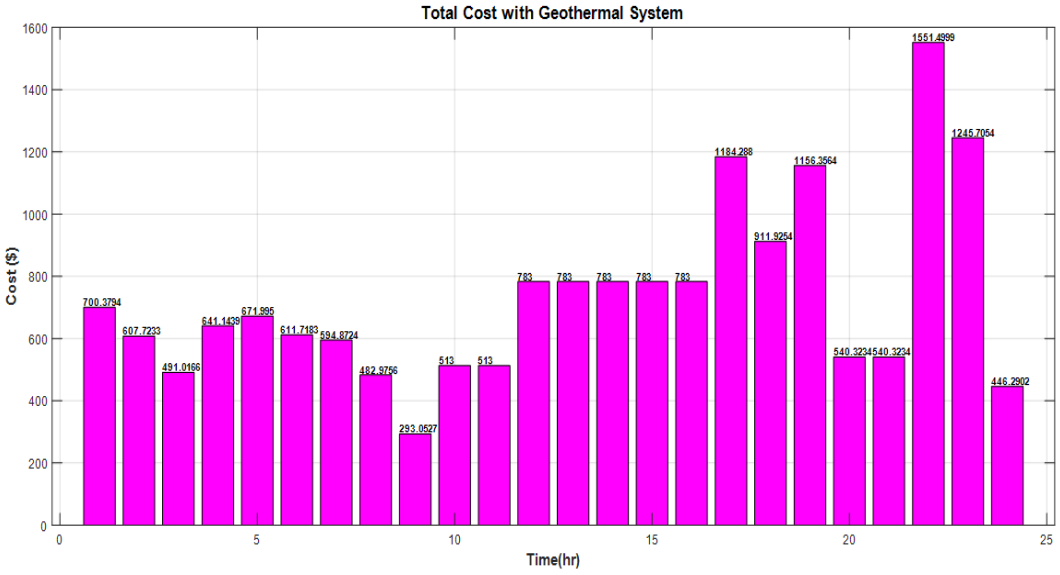

FIGURE 33. The total cost of PV-WT-BESS-DG utilizing GS in winter season.

GS and the other scenario using PV-WT-BESS and DG utilizing GS, as explained below.

a: SCENARIO (A): PV-WT-BESS UTILIZING GS

The result of MATLAB programming for total cost calculation in the winter season, shown in Figure 32, reveals that the total cost is reduced after using GS, which affects the power consumption of the load. This leads to a reduction in power drawn from the battery, which causes a decrease in cost value.

b: SCENARIO (B): PV-WT-BESS-DG UTILIZING GS

In this scenario, the total cost calculation for the winter season using all electrical power energy sources is shown in Figure 33. The figure shows that the total cost was reduced after using GS, which decreased the power consumption of the load, leading to a reduction in the power drawn from the battery, which caused a decrease in the cost value.

Comparing Figures 30 and 32, and Figures 31 and 33, it is evident that the total cost decreases when the electrical heating is turned on between 8 PM and 19 AM. It is clear that when utilizing a GS, the power consumption of electrical heating decreases. Compared to the case of not using a GS, this leads to a reduction in the cost of generating power sources and power savings.

VI. CONCLUSION

In conclusion, this study presented four scenarios for power generation to supply electrical loads. The generated power

sources (PV and WT) were connected to a BESS and DG utilizing a GS. Depending on the meteorological data of solar radiation, wind speed, and ambient temperature, the experimental data were measured on a sample day, July 13, in Basrah City in the southern region of Iraq. The power generation from batteries depends on their SOC, which is a considerable restriction that should be considered.

The previous scenarios show that not all loads are turned on when the first two scenarios focus on using only the PV-BESS and WT-BESS. It appears that the amount of power generated did not cover the power demand, while in scenario C, when using both sources of PV-WT with BESS, more residential loads could be turned on. Finally, all loads were turned on using the DG in scenario D. After calculating the total cost of the entire system, it is found to be significant. Thus, this study successfully used the addition of GS to reduce the total cost. It was found that the total cost decreased mainly when the air conditioner was turned on in summer or when the electrical heating was turned on in winter. This also leads to a reduction in emissions caused by the use of DG, in which CO_2 is the primary source of global climate change. It is widely recognized that to prevent the most severe effects of climate change, there is an urgent need to decrease CO_2 emissions globally. This paper presents an option for supplying residential home appliances in a remote area in Basrah City, a southern region of Iraq, using a hybrid system (PV-WT with BESS-DG utilizing a GS) with no grid connection. The actual data calculated for solar radiation and wind speed with the proposed load profile taken as a case study are presented. This study succeeded in programming and comparing multiple scenarios, finding the best choice for operation, and covering the load demand with minimum cost and emission reduction. The MATLAB program used in this study was adaptable. It can be modified to use other RE sources, such as hydro power and biogas, in any season or location (building, village, or city).

REFERENCES

[1] U. Akram, M. Khalid, and S. Shafiq, "An improved optimal sizing methodology for future autonomous residential smart power systems," *IEEE Access*, vol. 6, pp. 5986–6000, 2018.

[2] S. Kiros, B. Khan, S. Padmanaban, H. Haes Alhelou, Z. Leonowicz, O. P. Mahela, and J. B. Holm-Nielsen, "Development of stand-alone green hybrid system for rural areas," *Sustainability*, vol. 12, no. 9, p. 3808, May 2020.

[3] A. Al-Shereiqi, A. Al-Hinai, M. Albadi, and R. Al-Abri, "Optimal sizing of hybrid wind-solar power systems to suppress output fluctuation," *Energies*, vol. 14, no. 17, p. 5377, Aug. 2021.

[4] D. Fernández-Muñoz and J. I. Pérez-Díaz, "Optimisation models for the day-ahead energy and reserve self-scheduling of a hybrid wind–battery virtual power plant," *J. Energy Storage*, vol. 57, Jan. 2023, Art. no. 106296.

[5] S. Muhammad, T. Ali, Y. Khan, and M. Shafiullah, "Application of dynamic programming for optimal hybrid energy management system: Hydro-photovoltaic-diesel-BESS," *IEEE Access*, vol. 11, pp. 73767–73781, 2023.

[6] D. Velasco de la Fuente, C. L. Trujillo Rodríguez, G. Garcerá, E. Figueres, and R. Ortega Gonzalez, "Photovoltaic power system with battery backup with grid-connection and islanded operation capabilities," *IEEE Trans. Ind. Electron.*, vol. 60, no. 4, pp. 1571–1581, Apr. 2013.

[7] A. S. O. Ogunjuyigbe, T. R. Ayodele, and O. A. Akinola, "Optimal allocation and sizing of PV/wind/split-diesel/battery hybrid energy system for minimizing life cycle cost, carbon emission and dump energy of remote residential building," *Appl. Energy*, vol. 171, pp. 153–171, Jun. 2016.

[8] J. Zhang, H. Cho, R. Luck, and P. J. Mago, "Integrated photovoltaic and battery energy storage (PV-BES) systems: An analysis of existing financial incentive policies in the U.S.," *Appl. Energy*, vol. 212, pp. 895–908, Feb. 2018.

[9] M. Nurunnabi, N. K. Roy, E. Hossain, and H. R. Pota, "Size optimization and sensitivity analysis of hybrid wind/PV micro-grids—A case study for Bangladesh," *IEEE Access*, vol. 7, pp. 150120–150140, 2019.

[10] S. Moghaddam, M. Bigdeli, M. Moradlou, and P. Siano, "Designing of stand-alone hybrid PV/wind/battery system using improved crow search algorithm considering reliability index," *Int. J. Energy Environ. Eng.*, vol. 10, no. 4, pp. 429–449, Dec. 2019.

[11] A. B. Esan, A. F. Agbetuyi, O. Oghorada, K. Ogbeide, A. A. Awelewa, and A. E. Afolabi, "Reliability assessments of an islanded hybrid PV-diesel-battery system for a typical rural community in Nigeria," *Heliyon*, vol. 5, no. 5, May 2019, Art. no. e01632.

[12] A. A. Z. Diab, H. M. Sultan, I. S. Mohamed, O. N. Kuznetsov, and T. D. Do, "Application of different optimization algorithms for optimal sizing of PV/wind/diesel/battery storage stand-alone hybrid microgrid," *IEEE Access*, vol. 7, pp. 119223–119245, 2019.

[13] A. Razmjoo, R. Shirmohammadi, A. Davarpanah, F. Pourfayaz, and A. Aslani, "Stand-alone hybrid energy systems for remote area power generation," *Energy Rep.*, vol. 5, pp. 231–241, Nov. 2019.

[14] E. de Freitas Moscardini Júnior and R. Rüther, "The influence of the solar radiation database and the photovoltaic simulator on the sizing and economics of photovoltaic-diesel generators," *Energy Convers. Manage.*, vol. 210, Apr. 2020, Art. no. 112737.

[15] B. E. K. Nsafon, A. B. Owolabi, H. M. Butu, J. W. Roh, D. Suh, and J.-S. Huh, "Optimization and sustainability analysis of PV/wind/diesel hybrid energy system for decentralized energy generation," *Energy Strategy Rev.*, vol. 32, Nov. 2020, Art. no. 100570.

[16] N. Covic, F. Braeuer, R. McKenna, and H. Pandžic, "Optimal PV and battery investment of market-participating industry facilities," *IEEE Trans. Power Syst.*, vol. 36, no. 4, pp. 3441–3452, Jul. 2021.

[17] J. P. Medina and J. Lata-García, "Optimal model of a hybrid electrical system photovoltaic panel/wind turbine/battery bank, considering the feasibility of implementation in isolated areas," *J. Energy Storage*, vol. 36, Apr. 2021, Art. no. 102368.

[18] E. Mulenga, A. Kabanshi, H. Mupeta, M. Ndiaye, E. Nyirenda, and K. Mulenga, "Techno-economic analysis of off-grid PV-diesel power generation system for rural electrification: A case study of chilubi district in Zambia," *Renew. Energy*, vol. 203, pp. 601–611, Feb. 2023.

[19] M. Mikati, M. Santos, and C. Armenta, "Electric grid dependence on the configuration of a small-scale wind and solar power hybrid system," *Renew. Energy*, vol. 57, pp. 587–593, Sep. 2013.

[20] P. Sharma and T. S. Bhatti, "Performance investigation of isolated wind–diesel hybrid power systems with WECS having PMIG," *IEEE Trans. Ind. Electron.*, vol. 60, no. 4, pp. 1630–1637, Apr. 2013.

[21] R. A. Badwawi, M. Abusara, and T. Mallick, "A review of hybrid solar PV and wind energy system," *Smart Sci.*, vol. 3, no. 3, pp. 127–138, Jan. 2015.

[22] J. Sachs and O. Sawodny, "A two-stage model predictive control strategy for economic diesel-PV-battery island microgrid operation in rural areas," *IEEE Trans. Sustain. Energy*, vol. 7, no. 3, pp. 903–913, Jul. 2016.

[23] B. Mangu, S. Akshatha, D. Suryanarayana, and B. G. Fernandes, "Grid-connected PV-wind-battery-based multi-input transformer-coupled bidirectional DC–DC converter for household applications," *IEEE J. Emerg. Sel. Topics Power Electron.*, vol. 4, no. 3, pp. 1086–1095, Sep. 2016.

[24] Z. Yi, W. Dong, and A. H. Etemadi, "A unified control and power management scheme for PV-battery-based hybrid microgrids for both grid-connected and islanded modes," *IEEE Trans. Smart Grid*, vol. 9, no. 6, pp. 5975–5985, Nov. 2018.

[25] N. T. Mbungu, R. Naidoo, R. C. Bansal, and M. Bipath, "Optimisation of grid connected hybrid photovoltaic–wind–battery system using model predictive control design," *IET Renew. Power Gener.*, vol. 11, no. 14, pp. 1760–1768, 2017.

[26] Y. Sawle, S. C. Gupta, and A. K. Bohre, "Review of hybrid renewable energy systems with comparative analysis of off-grid hybrid system," *Renew. Sustain. Energy Rev.*, vol. 81, pp. 2217–2235, Jan. 2018.

[27] F. M. Gatta, A. Geri, S. Lauria, M. Maccioni, F. Palone, P. Portoghese, L. Buono, and A. Necci, "Replacing diesel generators with hybrid renewable power plants: Giglio smart island project," *IEEE Trans. Ind. Appl.*, vol. 55, no. 2, pp. 1083–1092, Mar. 2019.

[28] S. K. Tiwari, B. Singh, and P. K. Goel, "Control of wind–diesel hybrid system with BESS for optimal operation," *IEEE Trans. Ind. Appl.*, vol. 55, no. 2, pp. 1863–1872, Mar. 2019.

[29] T. García-Sánchez, A. K. Mishra, E. Hurtado-Pérez, R. Puché-Panadero, and A. Fernández-Guillamón, "A controller for optimum electrical power extraction from a small grid-interconnected wind turbine," *Energies*, vol. 13, no. 21, p. 5809, Nov. 2020.

[30] B. Singh, A. Verma, A. Chandra, and K. Al-Haddad, "Implementation of solar PV-battery and diesel generator based electric vehicle charging station," *IEEE Trans. Ind. Appl.*, vol. 56, no. 4, pp. 4007–4016, Jul. 2020.

[31] M. I. Juma, B. M. M. Mwinyiwiwa, C. J. Msigwa, and A. T. Mushi, "Design of a hybrid energy system with energy storage for standalone DC microgrid application," *Energies*, vol. 14, no. 18, p. 5994, Sep. 2021.

[32] A. Al-Quraan and M. Al-Qaisi, "Modelling, design and control of a standalone hybrid PV-wind micro-grid system," *Energies*, vol. 14, no. 16, p. 4849, Aug. 2021.

[33] F. Ez-zahra Lamzouri, E.-M. Boufounas, and A. E. Amrani, "Efficient energy management and robust power control of a stand-alone wind-photovoltaic hybrid system with battery storage," *J. Energy Storage*, vol. 42, Oct. 2021, Art. no. 103044.

[34] K. Thirugnanam, S. Kim Kerk, C. Yuen, N. Liu, and M. Zhang, "Energy management for renewable microgrid in reducing diesel generators usage with multiple types of battery," *IEEE Trans. Ind. Electron.*, vol. 65, no. 8, pp. 6772–6786, Aug. 2018.

[35] A. M. Eltamaly, M. A. Alotaibi, A. I. Alolah, and M. A. Ahmed, "A novel demand response strategy for sizing of hybrid energy system with smart grid concepts," *IEEE Access*, vol. 9, pp. 20277–20294, 2021.

[36] P. Liu, W. Zhao, J. Shair, J. Zhang, F. Li, P. Xv, and X. Xie, "Modeling of battery energy storage systems for AGC performance analysis in wind power systems," *Int. J. Electr. Power Energy Syst.*, vol. 155, Jan. 2024, Art. no. 109478.

[37] M. M. Gulzar, A. Iqbal, D. Sibtain, and M. Khalid, "An innovative converterless solar PV control strategy for a grid connected hybrid PV/wind/fuel-cell system coupled with battery energy storage," *IEEE Access*, vol. 11, pp. 23245–23259, 2023.

[38] R. Fan, Y. Jiang, Y. Yao, D. Shiming, and Z. Ma, "A study on the performance of a geothermal heat exchanger under coupled heat conduction and groundwater advection," *Energy*, vol. 32, no. 11, pp. 2199–2209, Nov. 2007.

[39] S. Nayak and G. N. Tiwari, "Theoretical performance assessment of an integrated photovoltaic and earth air heat exchanger greenhouse using energy and exergy analysis methods," *Energy Buildings*, vol. 41, pp. 888–896, Aug. 2009.

[40] A. Chel and G. N. Tiwari, "Stand-alone photovoltaic (PV) integrated with Earth to air heat exchanger (EAHE) for space heating/cooling of adobe house in New Delhi (India)," *Energy Convers. Manage.*, vol. 51, no. 3, pp. 393–409, Mar. 2010.

[41] P. M. Congedo, G. Colangelo, and G. Starace, "CFD simulations of horizontal ground heat exchangers: A comparison among different configurations," *Appl. Thermal Eng.*, vols. 33–34, pp. 24–32, Feb. 2012.

[42] F. Loveridge and W. Powrie, "Temperature response functions (G-functions) for single pile heat exchangers," *Energy*, vol. 57, pp. 554–564, Aug. 2013.

[43] S. Jakhar, R. Misra, V. Bansal, and M. S. Soni, "Thermal performance investigation of Earth air tunnel heat exchanger coupled with a solar air heating duct for northwestern India," *Energy Buildings*, vol. 87, pp. 360–369, Jan. 2015.

[44] S. K. Soni, M. Pandey, and V. N. Bartaria, "Ground coupled heat exchangers: A review and applications," *Renew. Sustain. Energy Rev.*, vol. 47, pp. 83–92, Jul. 2015.

[45] M. Kaushal, P. Dhiman, S. Singh, and H. Patel, "Finite volume and response surface methodology based performance prediction and optimization of a hybrid Earth to air tunnel heat exchanger," *Energy Buildings*, vol. 104, pp. 25–35, Oct. 2015.

[46] D. Wang, L. Lu, and P. Cui, "A new analytical solution for horizontal geothermal heat exchangers with vertical spiral coils," *Int. J. Heat Mass Transf.*, vol. 100, pp. 111–120, Sep. 2016.

[47] H. Boughanmi, M. Lazaar, A. Farhat, and A. Guizani, "Evaluation of soil thermal potential under Tunisian climate using a new conic basket geothermal heat exchanger: Energy and exergy analysis," *Appl. Thermal Eng.*, vol. 113, pp. 912–925, Feb. 2017.

[48] N. A. S. Elminshawy, A. M. I. Mohamed, K. Morad, Y. Elhenawy, and A. A. Alrobaian, "Performance of PV panel coupled with geothermal air cooling system subjected to hot climatic," *Appl. Thermal Eng.*, vol. 148, pp. 1–9, Feb. 2019.

[49] M. R. Naseh and E. Behdani, "Feasibility study for size optimisation of a geothermal/PV/wind/diesel hybrid power plant using the harmony search algorithm," *Int. J. Sustain. Energy*, vol. 40, no. 6, pp. 584–601, Jul. 2021.

[50] Ł. Amanowicz and J. Wojtkowiak, "Thermal performance of multi-pipe Earth-to-air heat exchangers considering the non-uniform distribution of air between parallel pipes," *Geothermics*, vol. 88, Nov. 2020, Art. no. 101896.

[51] S. F. Ahmed, G. Liu, M. Mofijur, A. K. Azad, M. A. Hazrat, and Y.-M. Chu, "Physical and hybrid modelling techniques for Earth-air heat exchangers in reducing building energy consumption: Performance, applications, progress, and challenges," *Sol. Energy*, vol. 216, pp. 274–294, Mar. 2021.

[52] M. Combe, A. Mahmoudi, M. H. Haque, and R. Khezri, "Cost-effective sizing of an AC mini-grid hybrid power system for a remote area in South Australia," *IET Gener., Transmiss. Distrib.*, vol. 13, no. 2, pp. 277–287, 2018.

[53] C. D. Korkas, S. Baldi, I. Michailidis, and E. B. Kosmatopoulos, "Occupancy-based demand response and thermal comfort optimization in microgrids with renewable energy sources and energy storage," *Appl. Energy*, vol. 163, pp. 93–104, Feb. 2016.

[54] Z. Chen and E. Spooner, "Grid power quality with variable speed wind turbines," *IEEE Trans. Energy Convers.*, vol. 16, no. 2, pp. 148–154, Jun. 2001.

[55] R. Jabbari-Sabet, S.-M. Moghaddas-Tafreshi, and S.-S. Mirhoseini, "Microgrid operation and management using probabilistic reconfiguration and unit commitment," *Int. J. Electr. Power Energy Syst.*, vol. 75, pp. 328–336, Feb. 2016.

[56] *Wind Speed and Solar Energy Database in Basrah-Iraq*, College of Engineering, Univ. Basrah, Basrah, Iraq, 2012.

[57] S. Abedi, A. Alimardani, G. B. Gharehpetian, G. H. Riahy, and S. H. Hosseinian, "A comprehensive method for optimal power management and design of hybrid RES-based autonomous energy systems," *Renew. Sustain. Energy Rev.*, vol. 16, no. 3, pp. 1577–1587, Apr. 2012.

[58] H. Yang, W. Zhou, L. Lu, and Z. Fang, "Optimal sizing method for stand-alone hybrid solar–wind system with LPSP technology by using genetic algorithm," *Sol. Energy*, vol. 82, no. 4, pp. 354–367, Apr. 2008.

[59] L. K. Gan, J. K. H. Shek, and M. A. Mueller, "Hybrid wind–photovoltaic–diesel–battery system sizing tool development using empirical approach, life-cycle cost and performance analysis: A case study in Scotland," *Energy Convers. Manage.*, vol. 106, pp. 479–494, Dec. 2015.

[60] B. Zhu, H. Tazvinga, and X. Xia, "Switched model predictive control for energy dispatching of a photovoltaic-diesel-battery hybrid power system," *IEEE Trans. Control Syst. Technol.*, vol. 23, no. 3, pp. 1229–1236, May 2015.

[61] R. Dufo-López, J. L. Bernal-Agustín, J. M. Yusta-Loyo, J. A. Domínguez-Navarro, I. J. Ramírez-Rosado, J. Lujano, and I. Aso, "Multi-objective optimization minimizing cost and life cycle emissions of stand-alone PV–wind–diesel systems with batteries storage," *Appl. Energy*, vol. 88, no. 11, pp. 4033–4041, Nov. 2011.

[62] S. H. Hammadi, "Tempering of water storage tank temperature in hot climates regions using Earth water heat exchanger," *Thermal Sci. Eng. Prog.*, vol. 6, pp. 157–163, Jun. 2018.

[63] H. Yang, Z. Wei, and L. Chengzhi, "Optimal design and techno-economic analysis of a hybrid solar–wind power generation system," *Appl. Energy*, vol. 86, no. 2, pp. 163–169, Feb. 2009.

[64] A. Yahiaoui, K. Benmansour, and M. Tadjine, "Optimal sizing and control strategy of renewable hybrid systems PV-diesel generator-battery: Application to the case of Djanet City of Algeria," *Adv. Sci., Technol. Eng. Syst. J.*, vol. 2, no. 3, pp. 485–491, 2017.

[65] S. H. Hammadi, "Freshwater production by combination of solar still, Earth-air heat exchanger and solar chimney for natural air draft," *Int. J. Sustain. Eng.*, vol. 14, no. 5, pp. 921–932, Sep. 2021.

[66] M. R. Nethra and B. Kalidasan, "Earth tube heat exchanger design for efficiency enhancement of PV panel," *Mater. Today: Proc.*, vol. 45, pp. 587–591, Jan. 2021.

[67] S. Bae and A. Kwasinski, "Dynamic modeling and operation strategy for a microgrid with wind and photovoltaic resources," *IEEE Trans. Smart Grid*, vol. 3, no. 4, pp. 1867–1876, Dec. 2012.
[68] M. Jahangiri, O. Nematollahi, A. Sedaghat, and M. Saghafian, "Techno-economical assessment of renewable energies integrated with fuel cell for off grid electrification: A case study for developing countries," *J. Renew. Sustain. Energy*, vol. 7, no. 2, 2015, Art. no. 023123.
[69] J. L. Bernal-Agustín, R. Dufo-López, and D. M. Rivas-Ascaso, "Design of isolated hybrid systems minimizing costs and pollutant emissions," *Renew. Energy*, vol. 31, no. 14, pp. 2227–2244, 2006.
[70] A. Janulevicius, A. Juostas, and A. Čiplienė, "Nitrogen-oxide emissions from diesel-engine farm tractors during real-life cycles and their correlation with the not-to-exceed operating zones," *Biosyst. Eng.*, vol. 161, pp. 93–105, Sep. 2017.
[71] F. Xiong, C. Zhu, G. Feng, J. Zheng, and H. Sun, "A three-dimensional coupled thermo-hydro model for geothermal development in discrete fracture networks of hot dry rock reservoirs," *Gondwana Res.*, vol. 122, pp. 331–347, Oct. 2023.

HIBA ABDULKAREEM KHAMIS was born in Basrah, Iraq, in 1984. She received the B.Sc. degree in electrical engineering from the Southern Technical University of Basrah, in 2006, and the M.Sc. degree in electrical engineering from the University of Basrah, in 2013. She is currently pursuing the Ph.D. degree with Shahid Chamran University of Ahvaz, Ahvaz, Iran, during the interspersed periods.

From 2007 to 2010, she was with the Technical Engineering College, Department of Electrical Engineering, Basrah. Since 2013, she has been an Assistant Lecturer and a Researcher with the Electrical Engineering Department, Technical Engineering College, Southern Technical University, Basrah. Her research interests include renewable energy sources, smart homes, smart grids, hybrid systems, and power management.

ELAHEH MASHHOUR (Member, IEEE) was born in Tehran, Iran, in 1974. She received the Ph.D. degree in electrical engineering from the K. N. Toosi University of Technology, Tehran, in 2010. She has worked at Khouzestan Electric Power Distribution Company for 15 years as the Manager of the network and load control office, the Manager of a power market office, and the Head of the DG participation unit. She has been an Associate Professor with the Department of Electrical Engineering, Shahid Chamran University of Ahvaz, Ahvaz, Iran, since 2011. Her research interests include distribution system automation and planning, power market, network resiliency, and deep learning.

MAHMOOD JOORABIAN received the M.S.C. degree in electrical power engineering from the Rensselaer Polytechnic Institute, Troy, NY, USA, in 1985, and the Ph.D. degree in electrical engineering from the University of Bath, Bath, U.K., in 1996. He is currently a Professor of electrical engineering with Shahid Chamran University of Ahvaz, Ahvaz, Iran. His research interests include power system modeling and applications of intelligence techniques to power system analysis, protection, and renewable energy (wind energy, design, and construction of ironless axial flux direct-drive generator for wind applications).

SEYYED GHODRATOLLAH SEIFOSSADAT was born in Ahvaz, Iran, in August 1963. He received the B.Sc. degree in electrical engineering from Iran University of Science and Technology (IUST), Tehran, Iran, in 1989, and the M.Sc. degree in electrical engineering from the Ferdowsi University of Mashhad, Mashhad, Iran, in 1992, and the Ph.D. degree from IUST, in 2006. He is currently a Professor with the Department of Electrical Engineering, Shahid Chamran University of Ahvaz, Iran, where he has been, since 1992. His research interests include power system protection and power quality.

SALMAN H. HAMMADI received the B.Sc., M.Sc., and Ph.D. degrees in mechanical engineering from the College of Engineering, University of Basrah, Iraq, in 1988, 1993, and 2007, respectively. He is currently a Professor of mechanical engineering with the College of Engineering, Basrah University, specializing in thermo mechanics. His research interests include renewable energy and the thermal performance of buildings.